JAERI-M
91-018

ION TEMPERATURE PROFILE ANALYSIS OF JT-60 PLASMA WITH ION TEMPERATURE GRADIENT MODE

February 1991

Hiroshi SHIRAI, Toshio HIRAYAMA and Masafumi AZUMI

日 本 原 子 力 研 究 所
Japan Atomic Energy Research Institute

JAERI-Mレポートは，日本原子力研究所が不定期に公刊している研究報告書です。
入手の問合わせは，日本原子力研究所技術情報部情報資料課（〒319－11茨城県那珂郡東海村）あて，お申しこしください。なお，このほかに財団法人原子力弘済会資料センター（〒319-11茨城県那珂郡東海村日本原子力研究所内）で複写による実費頒布をおこなっております。

JAERI-M reports are issued irregularly.
Inquiries about availability of the reports should be addressed to Information Division, Department of Technical Information, Japan Atomic Energy Research Institute, Tokai-mura, Naka-gun, Ibaraki-ken 319-11, Japan.

編集兼発行　日本原子力研究所
印　　　刷　日立高速印刷株式会社

Ion Temperature Profile Analysis of JT-60 Plasma with Ion Temperature Gradient Mode

Hiroshi SHIRAI, Toshio HIRAYAMA and Masafumi AZUMI

Department of Large Tokamak Research
Naka Fusion Research Establishment
Japan Atomic Energy Research Institute
Naka-machi, Naka-gun, Ibaraki-ken

(Received January 31, 1991)

Ion temperature profiles of neutral beam heated plasmas in JT-60 have been estimated by using ion thermal diffusivities, χ_i, based on the ion temperature gradient mode (η_i mode) turbulence theories and compared with experimental profiles measured by charge exchange recombination spectroscopy (CXRS). We have adopted three different χ_i models proposed by Dominguez & Waltz, Lee & Diamond, and Romanelli.

The calculated ion temperature profiles show good agreement with experimental data in the wide range of plasma parameter of L-mode discharges, which is I_p=1.0∿1.8MA, P_{abs}=1.3∿16.7MW, $\bar{n}_e$=1.2∿5.0×$10^{19}$$m^{-3}$ for the divertor discharges and I_p=2.0∿2.7MA, P_{abs}=3.0∿17.4MW, $\bar{n}_e$=1.5∿6.5×$10^{19}$$m^{-3}$ for the limiter discharges. Three different η_i mode models of χ_i do not show significant difference in this parameter range, when the proper choice of numerical factor of χ_i is employed. In the high ion temperature plasmas ($T_i(0) \geq 10$ keV), which were obtained under the condition of $I_p \leq 0.5$ MA and $P_{abs} \geq 15$MW, the calculated ion temperature profiles are broader than that of experiment. The large toroidal flow, or the velocity shear, may have an effect on the peaking of the ion temperature profile in these discharges besides the reduction of χ_i.

Keywords : Ion Temperature Profiles, JT-60, Plasma, Neutral Beam, Ion Temperature Gradient Mode

イオン温度勾配不安定性に基づく
ＪＴ－60プラズマのイオン温度分布解析

日本原子力研究所那珂研究所臨界プラズマ研究部
白井　浩・平山　俊雄・安積　正史

（1991年1月31日受理）

イオン温度勾配不安定性（η_iモード）に基づくイオン熱拡散係数χ_iを用いて，中性粒子入射加熱時におけるＪＴ－60プラズマのイオン温度分布を解析し，荷電交換再結合分光（ＣＸＳＲ）による測定値との比較をおこなった。本研究では，χ_iの理論値としては，Dominguez & Waltz，Lee & Diamond 及びRomanelliによって提唱されている３つの異なった表式を用いた。イオン温度分布の理論予測値は，イオン温度以外のプラズマ・パラメータにたいして実験値を用い，各χ_iモデルに対してイオンのエネルギー・バランス方程式を解くことによって求めた。

計算されたイオン温度分布理論予測値は，いずれも，Ｌモード放電の広範囲のプラズマ・パラメータ領域で実験値と良い一致を示した。解析した範囲は，ダイバータ放電では，$I_p = 1.0 \sim 1.8$ MA，$P_{abs} = 1.3 \sim 16.7$ MW，$\bar{n}_e = 1.2 \sim 5.0 \times 10^{19} m^{-3}$，および，リミター放電では，$I_p = 2.0 \sim 2.7$ MA，$P_{abs} = 3.0 \sim 17.4$ MW，$\bar{n}_e = 1.5 \sim 6.5 \times 10^{19} m^{-3}$である。３種類の$\chi_i$モデルによる計算結果は，数値係数をそれぞれ適切に選んだ場合，このパラメータ領域で顕著な差を示さなかった。一方，$I_p < 0.5$ MA，$P_{abs} > 15$ MWで得られた高イオン温度放電（$T_i(0) > 10$ keV）では，計算値は観測されたイオン温度分布ほどピークした分布を示さなかった。χ_iの改善以外にトロイダル流速，あるいは，その流速のシアーがピークしたイオン温度分布の形成に影響を与えている可能性もある。

那珂研究所：〒311-01　茨城県那珂郡那珂町大字向山801-1

Contents

目　　次

1. INTRODUCTION

In JT-60, transport analysis have been done both in ohmically heated and neutral beam heated plasmas. In the previous work [1], we calculated electron and ion temperature profiles by using a one dimensional tokamak transport code [2] with thermal diffusivities based on the drift wave turbulence. We assumed that the electron and ion thermal diffusivities were determined by trapped electron modes, circulation electron modes and ion temperature gradient modes (η_i modes). We compared the results of calculation with experimental data in the wide range of plasma parameters; the plasma current of I_p = 1.0 ~ 2.5 MA, the line averaged electron density of $\bar{n}_e = 1.0 \sim 8.0 \times 10^{19}$ m^{-3} and the neutral beam heating power of $P_{NBI} = 5 \sim 20$ MW in discharges with the outside X-point divertor and the limiter configurations

The calculated electron temperatures showed good agreement with the experimental data in the medium range of line averaged electron density $\bar{n}_e \sim 4.0 \times 10^{19}$ m^{-3} both in ohmically heated and neutral beam heated plasmas. On the other hand, this model underestimated both electron and ion temperatures in a low $\bar{n}_e$ regime and could not reproduce high temperature plasmas observed in neutral beam heating experiments.

The discrepancy between the calculated temperature and that of experimental data arises from the strong T_e dependence of thermal diffusivity, especially the thermal diffusivity induced by the dissipative trapped electron mode which has $T_e^{7/2}$ dependence. Since the effect of dissipative trapped electron mode was included in both electron and ion thermal diffusivity formulas, not only the electron temperature but also the ion temperature is strongly suppressed.

In these analysis, we calculated electron and ion temperatures simultaneously. In order to exclude the influence on calculation results in either side of calculated temperature (the electron temperature or the ion temperature) from the other side of calculated temperature which may deviate from the experimental data , it is better to analyze each temperature independently, that is, electron temperature only or ion temperature only, with all other plasma parameters fixed. In those days, however, there were noways to compare the calculated ion temperature profile with experimental data. Since 1988, the charge exchange recombination spectroscopy (CXRS) system [3] provides 8 spatial points of ion temperature data in the neutral beam heated plasmas.

In this paper, we concentrate ourselves on the analysis of the ion energy transport mainly in L-mode discharges heated by the neutral beam in lower X-point divertor and limiter configurations. We compare ion temperature profiles calculated from theoretical ion transport models with experimental results and check the validity of these models. We solve the ion temperature transport equation by using the χ_i models based on η_i mode turbulence, while other plasma parameters such as n_e, n_i, T_e, Z_{eff}, P_{rad} are fixed. We adopt three different χ_i models proposed by Dominguez & Waltz [4], Lee & Diamond [6], and Romanelli [7].

In the next section, we present the χ_i model based on η_i mode, trapped electron mode and circulating electron mode used in this paper. In section 3 and 4, the analysis of ion temperature profile in L-mode plasmas and high ion temperature plasmas are shown. In Section 5, summary of this paper and some problems are discussed.

2. MODEL OF CALCULATION

2.1 Model of Ion Thermal Diffusivities

We employ the formula of ion thermal diffusivity, χ_i, shown as follows;

$$\chi_i = \chi_i^{\eta_i} + \chi_i^{TE/CE} + \chi_i^{NC} \quad (1)$$

The first term in the RHS of equation (1) is the thermal diffusivity based on the η_i mode turbulence. The second term represents the edge transport model which is based on the trapped electron mode and the circulating electron mode [4]. The third term is Chang & Hinton's neoclassical diffusivity [8]. The first and the second terms are shown in detail in the following subsections. The following formula is also adopted for comparison,

$$\chi_i = \chi_i^{\eta_i} + \chi_i^{INTOR} + \chi_i^{NC}, \quad (2)$$

where χ_i^{INTOR} is the empirical thermal diffusivity of INTOR type.

2.2 Model of Ion Thermal Diffusivities by η_i Mode

We adopt three different types of χ_i models based on the η_i mode turbulence, whose formula are shown as follows;

(a) Dominguez & Waltz's model [4]

$$\chi_i^{D/W} = 2.5\, C^{\eta_i} \frac{\omega_{*e}}{k_\theta^2} \left(\frac{2 T_i L_n \eta_i}{T_e R} \right)^{1/2} f(\eta_i) \quad (3)$$

(b) Lee & Diamond's model [6]

$$\chi_i^{L/D} = 0.4\, C^{\eta_i} \left\{ \pi/2 \frac{T_i}{T_e} (1+\eta_i) \ln(1+\eta_i) \right\}^2 \frac{\rho_s^2 c_s}{L_s} f(\eta_i) \quad (4)$$

(c) Romanelli's model [7]

$$\chi_i^{R} = 3\, C^{\eta_i} \frac{v_i \rho_i^2}{L_n} \varepsilon_n^{1/2} (\eta_i - \eta_{ic})^{1/2} \quad (5)$$

where

$$\eta_i \equiv \frac{L_n}{L_{T_i}} = \frac{d \ln T_i}{dr} / \frac{d \ln n_e}{dr},$$

temperature profile in L-mode plasmas and high ion temperature plasmas are shown. In Section 5, summary of this paper and some problems are discussed.

2. MODEL OF CALCULATION

2.1 Model of Ion Thermal Diffusivities

We employ the formula of ion thermal diffusivity, χ_i, shown as follows;

$$\chi_i = \chi_i^{\eta_i} + \chi_i^{TE/CE} + \chi_i^{NC} \quad (1)$$

The first term in the RHS of equation (1) is the thermal diffusivity based on the η_i mode turbulence. The second term represents the edge transport model which is based on the trapped electron mode and the circulating electron mode [4]. The third term is Chang & Hinton's neoclassical diffusivity [8]. The first and the second terms are shown in detail in the following subsections. The following formula is also adopted for comparison,

$$\chi_i = \chi_i^{\eta_i} + \chi_i^{INTOR} + \chi_i^{NC}, \quad (2)$$

where χ_i^{INTOR} is the empirical thermal diffusivity of INTOR type.

2.2 Model of Ion Thermal Diffusivities by η_i Mode

We adopt three different types of χ_i models based on the η_i mode turbulence, whose formula are shown as follows;

(a) Dominguez & Waltz's model [4]

$$\chi_i^{D/W} = 2.5\, C^{\eta_i} \frac{\omega_{*e}}{k_\theta^2} \left(\frac{2T_i L_n \eta_i}{T_e R}\right)^{1/2} f(\eta_i) \quad (3)$$

(b) Lee & Diamond's model [6]

$$\chi_i^{L/D} = 0.4\, C^{\eta_i} \left\{ \pi/2 \frac{T_i}{T_e} (1+\eta_i) \ln(1+\eta_i) \right\}^2 \frac{\rho_s^2 c_s}{L_s} f(\eta_i) \quad (4)$$

(c) Romanelli's model [7]

$$\chi_i^{R} = 3\, C^{\eta_i} \frac{v_i \rho_i^2}{L_n} \varepsilon_n^{1/2} (\eta_i - \eta_{ic})^{1/2} \quad (5)$$

where

$$\eta_i \equiv \frac{L_n}{L_{T_i}} = \frac{d \ln T_i}{dr} \Big/ \frac{d \ln n_e}{dr},$$

$$L_n = n_e / \left|\frac{dn_e}{dr}\right|, \quad L_{T_i} = T_i / \left|\frac{dT_i}{dr}\right|, \quad L_s = R\, q^2 / r \frac{dq}{dr},$$

$$\omega_{*e} = \frac{k_\theta T_e}{L_n e B_t}, \quad \omega_{be} = \left(\frac{T_e}{m_e}\right)^{1/2} \frac{1}{qR}, \quad \rho_s = \frac{(m_i T_e)^{1/2}}{eB_t}, \quad \rho_i = \frac{(m_i T_i)^{1/2}}{eB_t},$$

$$C_s = \left(\frac{T_e}{m_i}\right)^{1/2}, \quad V_i = \left(\frac{T_i}{m_i}\right)^{1/2},$$

$$k_\theta = \frac{0.3}{\rho_s}, \quad \varepsilon_n = \frac{L_n}{R}$$

and

$$f(\eta_i) = \frac{1}{1 + \exp(-6(\eta_i - \eta_{ic}))} \tag{6}$$

The numerical coefficient, C^{η_i}, is set afterward. In this paper, we mainly adopt Dominguez & Waltz's model and other models are used for comparison. These three χ_i formula have the same temperature dependence of $T^{1.5}$, if T_e is close to T_i. The function $f(\eta_i)$ gives the smooth transition of χ_i around the threshold value, η_{ic}, of η_i. This function is almost zero below η_{ic} - 0.5 and almost one above η_{ic} + 0.5 (See Fig.1). In the Romanelli's model, we also slightly modify the η_i dependence on χ_i near the threshold ($\eta_{ic} - 0.4 \le \eta_i \le \eta_{ic} + 0.2$) in order to avoid the numerical problems arising from the large value of $\partial\chi_i/\partial\eta_i$ near $\eta_i = \eta_{ic}$ in the original formula. Figure 2 shows comparison of the original η_i dependence on χ_i of Romanelli's model (broken line) and the modified one used in the following calculations (solid line).

The value of η_{ic} is determined as follows [7],[9];

$$\eta_{ic} = \eta_{ic}(\varepsilon_n) = \begin{cases} 1 & (\varepsilon_n \le 0.2) \\ 1 + 2.5\,(\varepsilon_n - 0.2) & (\varepsilon_n \ge 0.2) \end{cases} \tag{7}$$

This formula indicates that η_{ic} becomes large where the density profile is flat; that is, near the plasma central region. The unstable region against η_i mode by this η_{ic} model is shown in Fig.3 by (L_{T_i}, L_n) space. We will compare the results of calculation with the constant η_{ic} case; $\eta_{ic} = 1$, in Section 3.

2.3 Model of Plasma Edge Transport

In equation (1), $\chi_i^{TE/CE}$ represents thermal diffusivity contributed from trapped electron mode, χ_i^{TE}, and circulating electron mode, χ_i^{CE} [4], that is;

$$\chi_i^{TE/CE} = C^{TE} \chi_i^{TE} + C^{CE} \chi_i^{CE} \tag{8}$$

χ_i^{TE} is made up of the collisionless trapped electron mode and the dissipative trapped electron mode

$$\chi_i^{TE} = \frac{5}{2}\frac{\omega_{*e}}{k_\theta^2}\varepsilon^{1/2}\min\left(1, \frac{\omega_{*e}\,\varepsilon}{\nu_{ei}}\right) \tag{9}$$

The value of χ_i^{TE} decreases toward the plasma center since the collisionless trapped electron mode and the dissipative trapped electron mode have L_n^{-1} and L_n^{-2} dependence in their formula, respectively. χ_i^{CE} is made up of the collisionless circulating electron mode and the collisional circulating electron mode,

$$\chi_i^{CE} = \frac{5}{2}\frac{\omega_{*e}^2}{k_\theta^2\,\omega_{bc}}\max\left(1, \frac{\nu_{ei}}{\omega_{be}}\right) \tag{10}$$

The value of χ_i^{CE} also decreases toward the plasma center; more drastically comparing with the trapped electron modes. These modes have L_n^{-2} dependence in their formula and is large only very near the plasma surface. The second term in the RHS of equation (2) is defined as

$$\chi_i^{INTOR} = C^{INTOR}\frac{5\times10^{19}}{n_e} \tag{11}$$

Coefficients such as C^{TE}, C^{CE} and C^{INTOR} are set afterward.

2.4 Methods of Calculation

We obtain the radial profiles of plasma parameters such as n_e, T_e and T_i from the diagnostic data at discrete radial points by using the least square fitting method. We adopt following two types of fitting function:

(i) Parabolic fitting function

$$f(r,\alpha) = (f(0)-f(1))\,(1-r^2)^\alpha + f(1) \tag{12}$$

(ii) Pedestal fitting function

$$f(r,\alpha,\beta) = (f(0)-f(1))\left\{1 - r^2 + \alpha r^2(1-r^2) + \beta r^2(1-r^4)\right\} + f(1) \tag{13}$$

f(0) and f(1) are the central and boundary values respectively. Coefficients such as α and β are determined by the least square method.

The effective charge number, Z_{eff}, measured by the visible Bremsstrahlung is assumed to be spatially constant. The fast ion density profile, n_i^f, is calculated by Orbit-Following-Monte Carlo Code (OFMC code)[10]. The thermal ion density, n_i^{th}, is then calculated as $n_i^{th} = n_i - n_i^f$. The neutral density profile is calculated by using the Monte Calro technique and the absolute value of neutral density is evaluated from the particle confinement time obtained by the empirical scaling law. The power deposition profile of neutral beam to electrons, P_{NBI}^e and to ions, P_{NBI}^i, are also calculated by OFMC. As for the plasma current profile, we set $J(r) = J(0)\,(1 - r^2)^{q(1)-1}$ assuming $q(0) = 1$.

For these plasma parameters, the ion temperature profile is calculated from the steady state equation of ion energy balance with prescribed theoretical models of χ_i. The calculated ion temperature profile is compared with experimental data.

2.5 Thermal Diffusivity Calculated by Experimental Data Analysis

In the following section, we compare the profile of theoretical χ_i model with that obtained from the experimental data analysis of the measured T_i profile. We express the latter as χ_i^{Scoop} which is defined as follows;

$$\chi_i^{Scoop}(r) = \frac{-\frac{3}{2} T_i \Gamma_i + \frac{1}{r < |\nabla r|^2 >} \int_0^r (- P_{CX} - P_{eq} + P_{NBI}^i)\, r\, dr}{- n_i \frac{\partial T_i}{\partial r}} \tag{14}$$

where Γ_i, P_{CX} and P_{eq} represent the ion particle flux, the charge exchange loss and the equi-partition energy exchange between electrons and ions, respectively. Γ_i, is defined as follows.

$$\Gamma_i (r) = \frac{1}{r \langle |\nabla r|^2 \rangle} \int_0^r dr\, r\, (S_n + S_{NB}) , \tag{15}$$

where S_n and S_{NB} are a local particle source inferred from a particle confinement time and a fast ion birth profile of neutral beam calculated by the OFMC code, respectively. The particle confinement time is assumed by an empirical scaling of τ_p (sec) = 0.05 / $\bar{n}_e(10^{20}m^{-3})$ / $P_{abs}(MW)^{0.5}$, where $\bar{n}_e$ is the line average density and P_{abs} totally absorbed heating power.

3. RESULTS OF CALCULATION IN L-MODE PLASMAS

In this section, we calculate T_i profiles of neutral beam heated, L-mode plasmas in JT-60 by using the transport models described in the previous section. At first, we compare the calculated T_i profiles with and without the second term of RHS of eq.(1). In the calculation hereafter, we employ two sets of coefficients in eq.(1) ;

case (I) $C^{\eta_i} = 0.6$, $C^{TE} = 0$. and $C^{CE} = 0$,

and

case (II) $C^{\eta_i} = 0.5$, $C^{TE} = 0.2$ and $C^{CE} = 0.2$.

We adopt the Dominguez & Waltz's χ_i model. These sets of coefficients are determined to adjust the calculated ion temperature profile to the experimental data of typical 1.0 MA and 1.5 MA divertor shots.

We select the shot number E10737 (P_{abs} = 11.1 MW, $\bar{n}_e = 2.9 \times 10^{19}$ m^{-3}, Z_{eff} = 3.5) as the typical discharge in the 1.5 MA lower X-point divertor configuration. The profile

For these plasma parameters, the ion temperature profile is calculated from the steady state equation of ion energy balance with prescribed theoretical models of χ_i. The calculated ion temperature profile is compared with experimental data.

2.5 Thermal Diffusivity Calculated by Experimental Data Analysis

In the following section, we compare the profile of theoretical χ_i model with that obtained from the experimental data analysis of the measured T_i profile. We express the latter as χ_i^{Scoop} which is defined as follows;

$$\chi_i^{Scoop}(r) = \frac{-\frac{3}{2} T_i\Gamma_i + \frac{1}{r < |\nabla r|^2 >} \int_0^r (- P_{CX} - P_{eq} + P_{NBI}^i) \, r \, dr}{- n_i \frac{\partial T_i}{\partial r}} \tag{14}$$

where Γ_i, P_{CX} and P_{eq} represent the ion particle flux, the charge exchange loss and the equi-partition energy exchange between electrons and ions, respectively. Γ_i, is defined as follows.

$$\Gamma_i (r) = \frac{1}{r\langle|\nabla r|^2\rangle} \int_0^r dr \, r \, (S_n + S_{NB}) , \tag{15}$$

where S_n and S_{NB} are a local particle source inferred from a particle confinement time and a fast ion birth profile of neutral beam calculated by the OFMC code, respectively. The particle confinement time is assumed by an empirical scaling of τ_p (sec) = 0.05 / $\bar{n}_e(10^{20}m^{-3})$ / $P_{abs}(MW)^{0.5}$, where $\bar{n}_e$ is the line average density and P_{abs} totally absorbed heating power.

3. RESULTS OF CALCULATION IN L-MODE PLASMAS

In this section, we calculate T_i profiles of neutral beam heated, L-mode plasmas in JT-60 by using the transport models described in the previous section. At first, we compare the calculated T_i profiles with and without the second term of RHS of eq.(1). In the calculation hereafter, we employ two sets of coefficients in eq.(1) ;

case (I) $C^{\eta_i} = 0.6$, $C^{TE} = 0$ and $C^{CE} = 0$,

and

case (II) $C^{\eta_i} = 0.5$, $C^{TE} = 0.2$ and $C^{CE} = 0.2$.

We adopt the Dominguez & Waltz's χ_i model. These sets of coefficients are determined to adjust the calculated ion temperature profile to the experimental data of typical 1.0 MA and 1.5 MA divertor shots.

We select the shot number E10737 (P_{abs} = 11.1 MW, $\bar{n}_e = 2.9 \times 10^{19}$ m^{-3}, Z_{eff} = 3.5) as the typical discharge in the 1.5 MA lower X-point divertor configuration. The profile of plasma parameters of this shot such as n_e, n_i, n_i^{th}, T_e, P_{NBI}^e and P_{NBI}^i are shown in Fig.4. The χ_i profile of case (I) is shown in Fig.5(a). The thin solid line is the contribution from the η_i mode, χ^{η_i}, and the dotted line corresponds to the neoclassical diffusion, χ^{NC}. The thick solid line is the sum of them, χ_i^{Total}. We can see that χ^{η_i} is the dominant term in the core plasma. Since χ^{η_i} has the temperature dependence of $T_e\, T_i^{0.5}$, it decreases toward the plasma edge region. The χ^{NC} is about one order smaller than χ^{η_i} and becomes comparable to χ^{η_i} only very near the magnetic axis where χ^{NC} increases as $\varepsilon^{-1.5}$. Fig.5(b) is the χ_i profile of case (II). The broken line is the contribution from trapped electron modes and circulating electron modes, $\chi_i^{TE/CE}$. Other lines are the same as in Fig.5(a). The value of $\chi_i^{TE/CE}$ is large in the plasma peripheral region, where the main contribution comes from circulating electron modes, χ_i^{CE}. Apart from the plasma periphery, the χ_i^{CE} value decreases rapidly and the contribution from trapped electron modes, χ_i^{TE}, takes its place. Because the $\chi_i^{TE/CE}$ decreases toward plasma center, the η_i mode turbulence is still the dominant conduction loss mechanism in the core plasma as in the case (I).

Figure 5(c) is the comparison of η_{ic} (eq.(7); broken line) and η_i values of case (I) (dotted line) and case(II) (solid line). Except for the plasma center, both η_i are larger than η_{ic}. At $r \sim 0.4$ m where the density gradient is small, the η_i values become somewhat larger than that of other region. Figure 5(d) is the comparison of χ_i^{Total} of case (I) (dotted line) and case(II) (solid line) with χ_i^{Scoop} (broken line) calculated by experimental data analysis (eq.(14)). The calculated χ_i of case (II) agrees well with χ_i^{Scoop}. The calculated χ_i of case (I) also agrees with χ_i^{Scoop} except in the plasma peripheral region.

Figure 5(e) shows the calculated T_i profile of case (I) (dotted line) and (II) (solid line) and experimental data measured by CXRS. It is interesting to see that the calculated ion temperature profile in the case (I) agrees with experimental data in spite of the discrepancy of calculated χ_i value with χ_i^{Scoop} in the plasma peripheral region. In the case (II), better agreement of calculated T_i profile with experimental data can be seen.

The reason why the deviation of calculated χ_i from χ_i^{Scoop} in the plasma peripheral region does not make so much difference in the T_i profile between the calculation and the experimental data is apparent from Fig.6. This figure shows the ion energy flow integrated from the plasma center of each case (Fig.6(a) for case (I) and Fig.6(b) for case (II)). In this figure, the thin solid line, the thick solid line, the broken line, the dotted line and the dotted-broken line are the neutral beam heating power, conduction loss, convection loss, charge exchange loss and the equi-partition between electrons and ions, respectively. The dominant loss channel in the core plasma is the conduction loss. In the plasma peripheral region, however, the equi-partition loss or convection loss becomes comparable to or greater than the conduction loss. For this reason, the difference between theoretical χ_i and χ_i^{Scoop} in the plasma peripheral region weakly affects the T_i profile.

We tried the comparison of calculated T_i profile with experimental data for both case (I) and (II) in several shots. The calculated T_i profiles for both cases agree with experimental data. The $\chi_i^{TE/CE}$ term in eq.(1) affects the T_i profile only near the plasma peripheral region in the parameter range of the L-mode discharges. The T_i profile of case (I) is slightly fat at the plasma edge region comparing with case (II). Since the better agreement of calculation and experimental data can be seen in case (II), we study the plasma current dependence and the absorption power dependence of transport characteristics with coefficients of case (II) hereafter.

Figure 7 shows the comparison of calculated T_i profiles with experimental data in the different plasma current; (a) 1.0 MA, (b) 1.8 MA, (c) 2.0 MA and (d) 2.7 MA. The case (a),(b) and (c),(d) are divertor and limiter shots, respectively. The absorption power range is 9.7 ~ 12.1 MW . The solid line is the calculated T_i profile. Good agreement of calculated T_i and experimental data can be seen.

Next, we show the comparison of calculated T_i profiles with experimental data for different absorption powers. They are shown in Fig.8 (1.0 MA divertor shots), Fig.9 (1.5 MA divertor shots), Fig.10 (2.0 MA limiter shots) and Fig.11 (2.7 MA limiter shots). The calculated T_i profiles shown in solid line agree well with experimental data in the wide range of plasma parameters; $I_p = 1.0 \sim 1.8$ MA, $P_{abs} = 1.3 \sim 16.7$ MW, $\bar{n}_e = 1.2 \sim 5.0 \times 10^{19}$ m^{-3} for the lower X-point divertor shots and $I_p = 2.0 \sim 2.7$ MA, $P_{abs} = 3.0 \sim 17.4$ MW, $\bar{n}_e = 1.5 \sim 6.5 \times 10^{19}$ m^{-3} for the limiter shots. For these shots, the line averaged electron density is not always in the same range because the change of neutral beam heating power accompanies the change of electron density, especially in limiter discharges.

The comparison of ion stored energy obtained by the calculation above and that of experimental data are compared in Fig.12. They show good agreement except for some 1.0 MA limiter shots. The results of 1.0 MA limiter case is presented afterward.

We have obtained the similar calculation results by using other theoretical χ_i models based on the η_i mode turbulence, mentioned in the section 2.2. Figure 13 is the calculation results of typical shot E10737 by Lee & Diamond's χ_i model (eq.(4)), in which we set $C^{\eta_i} = 2.5$, $C^{TE} = 0.2$ and $C^{CE} = 0.2$. This χ_i model has strong dependence on η_i value and the difference between η_{ic} and the calculated η_i is not so large everywhere (0.7 at the utmost), different from the Dominguez & Waltz's model. Since Lee & Diamond's model has L_s^{-1} dependence, the χ_i value decreases toward the plasma center. As the result, the calculated χ_i has the somewhat convex shape comparing with χ_i^{Scoop}. However the calculated T_i profile agrees well with experimental data within their error bars.

Figure 14 is the calculation results of Romanelli's χ_i model (eq.(5)), in which we set $C^{\eta_i} = 0.8$, $C^{TE} = 0.2$ and $C^{CE} = 0.2$. The χ_i show the similar radial profile as χ_i^{Scoop} and the calculated T_i agrees well with experimental T_i profile in the whole plasma region. We also obtained good agreement of calculated T_i and experimental data in other shots with using the same coefficients mentioned above.

In the 1.0 MA limiter shots, the calculated T_i profile by the η_i mode turbulence models used above becomes much larger than experimental data. For example, we show the typical 1.0 MA limiter shot case (E10619, $P_{abs} = 5.58$ MW, $\bar{n}_e = 1.67 \times 10^{19}$ m^{-3} , $Z_{eff} = 3.5$). The profiles of n_e , n_i, n_i^{th}, T_e, P_{NBI}^e and P_{NBI}^i are shown in Fig.15. We use the Dominguez & Waltz's η_i mode model. Figure 16(a) shows the profile of η_{ic} and the calculated η_i. Figure 16(b) shows the profile of calculated χ_i and its composition. We can see that the η_i mode is the dominant conduction loss. The comparison of calculated χ_i with χ_i^{Scoop} and the comparison of calculated T_i with experimental data are shown in Fig.16(c) and (d). The value of calculated χ_i becomes lower than χ_i^{Scoop}, which gives rise to higher value of calculated T_i comparing with experiment.

In order to realize the degree of difference between the calculation and the experimental data, we compare the calculated T_i profile by changing coefficients such as C^{η_i}. Figure 17 shows the result. The solid line, the broken line and the dotted line indicate the case of (C^{η_i}, C^{TE}, C^{CE}) = (0.5, 0.2, 0.2), (1.0, 0.4, 0.4) and (2.0, 0.8, 0.8) respectively. The increase of transport coefficients by factor 4 makes agreement of calculated T_i and the experimental data. Results of other two 1.0 MA limiter shots also indicate that the calculated T_i is higher than experimental data.

We suppose two possibility to explain this. One is that local χ_i strongly depends on I_p in the limiter plasmas while weakly depends on I_p in the divertor plasmas. Actually, the global energy confinement time, τ_E, is proportional to $I_p^{0.74}$ in the limiter plasmas, which is stronger dependence than the case of lower X-point divertor plasmas in which τ_E is proportional to $I_p^{0.39}$ [11]. Of course it is uncertain whether both electron and ion transport equally depend on I_p in the limiter. However, if this is the case, the χ_i model mentioned above cannot explain the experimental T_i because there is essentially no I_p dependence in the χ_i formula in the models used above.

The other possibility is that because the Z_{eff} values are large (~ 4)in these limiter shots, the ion density dilution affects the calculation results. For example, if carbon is supposed to be the dominant impurity species in the plasma, the ion density in the $Z_{eff} = 3$ plasma is 50% larger than that of $Z_{eff} = 4$ plasma. In order to evaluate the effect of Z_{eff} on the calculation results, we calculate the same shot again changing the Z_{eff} value. In Fig. 18, the solid line, the broken line and the dotted line indicate the case of Z_{eff} = 3.0, 2.0 and 1.5 respectively. The decrease of Z_{eff} value accompanies the decrease of calculated T_i and better agreement with experimental data.

At the present time, there are only three 1.0 MA data available and the much impurity background in the limiter case degrades the precision of T_i measurement. We cannot definitely conclude on this matter.

4. RESULTS OF CALCULATION IN HIGH-TI PLASMAS

In this section, we analyze high ion temperature (high T_i) plasmas with the central ion temperature around 10 KeV or larger. These plasmas are obtained in the high power neutral beam heated case ($P_{abs} \geq 15$ MW) with low plasma current; $I_p \leq 0.5$ MA. We select the shot number E10300 (E10300, $I_p = 0.57$ MA, $P_{abs} = 15$ MW, $\bar{n}_e = 3.49 \times 10^{19}$ m^{-3} , $Z_{eff} = 2.82$) for the typical high T_i case. The profiles of n_e, n_i, n_i^{th}, T_e, P_{NBI}^e and P_{NBI}^i are shown in Fig.19.

The characteristics of high T_i shot is that the n_e profile as well as the T_i profile is highly central peaked pedestal profile. Still more, the T_i value in the region of $\frac{r}{a} \geq 0.5$ is very low. Especially in the $I_p = 0.3$ MA case, T_i value is 1 ~ 2 keV at $\frac{r}{a}$ ~ 0.5 whereas the central T_i value is about 10 keV. It is as if there are two different plasmas; the peaked profile and very high temperature central plasma and the low temperature edge plasma.

and (d). The value of calculated χ_i becomes lower than χ_i^{Scoop}, which gives rise to higher value of calculated T_i comparing with experiment.

In order to realize the degree of difference between the calculation and the experimental data, we compare the calculated T_i profile by changing coefficients such as C^{η_i}. Figure 17 shows the result. The solid line, the broken line and the dotted line indicate the case of (C^{η_i}, C^{TE}, C^{CE}) = (0.5, 0.2, 0.2), (1.0, 0.4, 0.4) and (2.0, 0.8, 0.8) respectively. The increase of transport coefficients by factor 4 makes agreement of calculated T_i and the experimental data. Results of other two 1.0 MA limiter shots also indicate that the calculated T_i is higher than experimental data.

We suppose two possibility to explain this. One is that local χ_i strongly depends on I_p in the limiter plasmas while weakly depends on I_p in the divertor plasmas. Actually, the global energy confinement time, τ_E, is proportional to $I_p^{0.74}$ in the limiter plasmas, which is stronger dependence than the case of lower X-point divertor plasmas in which τ_E is proportional to $I_p^{0.39}$ [11]. Of course it is uncertain whether both electron and ion transport equally depend on I_p in the limiter. However, if this is the case, the χ_i model mentioned above cannot explain the experimental T_i because there is essentially no I_p dependence in the χ_i formula in the models used above.

The other possibility is that because the Z_{eff} values are large (~ 4)in these limiter shots, the ion density dilution affects the calculation results. For example, if carbon is supposed to be the dominant impurity species in the plasma, the ion density in the Z_{eff} = 3 plasma is 50% larger than that of Z_{eff} = 4 plasma. In order to evaluate the effect of Z_{eff} on the calculation results, we calculate the same shot again changing the Z_{eff} value. In Fig. 18, the solid line, the broken line and the dotted line indicate the case of Z_{eff} = 3.0, 2.0 and 1.5 respectively. The decrease of Z_{eff} value accompanies the decrease of calculated T_i and better agreement with experimental data.

At the present time, there are only three 1.0 MA data available and the much impurity background in the limiter case degrades the precision of T_i measurement. We cannot definitely conclude on this matter.

4. RESULTS OF CALCULATION IN HIGH-TI PLASMAS

In this section, we analyze high ion temperature (high T_i) plasmas with the central ion temperature around 10 KeV or larger. These plasmas are obtained in the high power neutral beam heated case ($P_{abs} \geq 15$ MW) with low plasma current; $I_p \leq 0.5$ MA. We select the shot number E10300 (E10300, I_p = 0.57 MA, P_{abs} = 15 MW, $\bar{n}_e = 3.49 \times 10^{19}$ m^{-3} , Z_{eff} = 2.82) for the typical high T_i case. The profiles of n_e, n_i, n_i^{th}, T_e, P_{NBI}^e and P_{NBI}^i are shown in Fig.19.

The characteristics of high T_i shot is that the n_e profile as well as the T_i profile is highly central peaked pedestal profile. Still more, the T_i value in the region of $\frac{r}{a} \geq 0.5$ is very low. Especially in the I_p = 0.3 MA case, T_i value is 1 ~ 2 keV at $\frac{r}{a}$ ~ 0.5 whereas the central T_i value is about 10 keV. It is as if there are two different plasmas; the peaked profile and very high temperature central plasma and the low temperature edge plasma.

Figure 20(a) indicates the profile of η_{ic} and the calculated η_i value. In the plasma center, the η_i value becomes less than unity, which means the stabilization of η_i mode. The calculated η_i value takes maximum value at $\frac{r}{a} \sim 0.5$ where the density gradient is small. Figure 20(b)is the profile of calculated χ_i and its content. Since the electron temperature is high ($T_e(0) \sim 6$ keV), the χ_i contribution from the trapped electron mode becomes large at the plasma central region. This causes the flattening of ion temperature in the plasma central region and η_i value decreases below η_{ic}.

Figure 20(c) shows the comparison of the calculated χ_i with χ_i^{Scoop}. They considerably disagree. The calculated χ_i is almost constant in the plasma. On the other hand, the χ_i^{Scoop} is very low in the plasma center; almost the same as neoclassical value, and very large at the peripheral region. This is apparent from the experimental T_i profile and the formula of eq.(14). In the high T_i shots, the temperature gradient is very large in the plasma center region and is very small, nearly zero gradient, in the peripheral region. This results in the χ_i^{Scoop} profile shown in Fig.20(c). The similar profile of χ_i^{Scoop} is seen in other high T_i shots. For this reason, the calculated T_i profile becomes broader than experimental data (Fig.20(d)).

Even in the calculation without the trapped electron mode model in order to avoid its strong effect on the χ_i in the plasma central region where T_e is very high, we get similar calculation results which are shown in Fig.21. Three figures indicate the profile of (a) calculated η_i, and η_{ic} (b) calculated χ_i and (c) comparison of calculated T_i and experimental data. The solid line, broken line and dotted-broken line shown on each figure are the results of χ_i model by Dominguez & Waltz, Lee & Diamond and Romanelli respectively. Coefficients C^{η_i} are the same as that we use in the previous section. We can see that the role of the trapped electron mode is replaced by the η_i mode. Among three models, Lee & Diamond's model reproduce more peaked T_i profile comparing with the other models because calculated χ_i becomes convex profile similar to χ_i^{Scoop}. However, it is less peaked than experimental data.

Since the discrepancy between the calculated T_i and the experimental data is large in the plasma peripheral region, next we investigate whether η_i mode model is applicable at least in the plasma central region ($\frac{r}{a} \leq 0.5$) where the gradient of density and ion temperature is large. In order to reproduce the low ion temperature region in the plasma edge, we define the ion thermal diffusivity as follows;

$$\chi_i = \max\left(\chi_i^{\eta_i} + \chi_i^{\text{Neoclassical}}, \chi_i^{\text{Scoop}} \right) \tag{16}$$

Since the χ_i^{Scoop} value in the high plasma is very large in the plasma edge region, we can study the η_i mode transport only in the plasma central region. Figure 22 shows the profile of the calculated χ_i and T_i profiles. The calculated central T_i value is smaller than the experimental data.

After all, the T_i profile calculated by η_i mode model does not agree with the pedestal and center peaked T_i profile of high T_i shots. Other transport mechanism, for example inward heat pinch in the plasma central region which may be caused by the negative potential in the plasma central region, must be considered to explain the experimental data.

5. SUMMARY AND DISCUSSION

We investigate the effect of η_{ic} model on the calculation results. We compare the four constant η_{ic} models with $\eta_{ic} = -\infty$, 1, 1.5 and 2. The case of $\eta_{ic} = -\infty$ means that η_i mode is always destabilized. The results of Romanelli's η_{ic} model presented in the section 3 and 4 is almost the same with the $\eta_{ic} = 1$ case. Since the calculation with the same C^{η_i} value all through the different η_{ic} value results in the considerably different central ion temperature, the C^{η_i} value is adjusted for each η_{ic} case in order to, at least, reproduce the central ion temperature of experiment. In the Dominguez & Waltz's model, we set C^{η_i} values as 0.5, 0.5, 0.6 and 2.0 for the case of $\eta_{ic} = -\infty$, 1, 1.5 and 2, respectively. In the Lee & Diamond's model, we set them 2.5, 2.5, 3, 10.

Figure 23(a) is the comparison of η_i profile by these models for the discharge of E10737. We adopted Dominguez & Waltz's χ_i model. The solid line, broken line, dotted-broken line and the dotted line indicate the cases of $\eta_{ic} = -\infty$, 1, 1.5 and 2. In the $\eta_{ic} = -\infty$ case, the η_i value becomes maximum at r ~ 0.4 m where the L_n takes maximal value. Apart from r ~ 0.4 m, the η_i value deceases and is almost one at the plasma center and the edge region. As the η_{ic} value increases, the η_i value of plasma center and edge region increases whereas it deceases at r ~ 0.4 m. As a result, the η_i profile becomes flatter as the increase of η_{ic} value. Figure 23(b) shows the comparison of $f(\eta_i)$ profile (eq.(6)) for these models. As the η_{ic} value increases, the $f(\eta_i)$ value becomes smaller because the η_i mode is easier to be stabilized with high η_{ic} value. Figure 23(c) shows the calculated χ_i profiles. In spite of the different value and shape of $f(\eta_i)$ for each model, the obtained χ_i profile becomes similar because of the different C^{η_i} value. As a result, the calculated T_i profiles (Fig.23(d)) are almost the same and agree well with experimental data.

The reason why the η_i value at r ~ 0.4 m decrease as the increase of η_{ic} is as follows: As the η_{ic} value increase, the η_i mode tends to be stabilized at the plasma center and the edge region in the first place, where originally the η_i value is small. This results in the decrease of χ_i in this area. Since the C^{η_i} value is adjusted to reproduce the central T_i value, the χ_i value other than this area increase, especially around r ~ 0.4 m where the η_i value is originally large and it is harder to stabilize η_i mode, and the ion temperature gradient around r ~ 0.4 m is compelled to be decreased. As a result, the η_i value at r ~ 0.4 m decrease. In short, the increase of both η_{ic} and C^{η_i} makes flatter η_i profile as the increase of η_{ic}.

We made the same calculation with Lee & Diamond's χ_i model. They are shown in Fig.24. Since the Lee & Diamond's χ_i formula has L_s^{-1} dependence, which becomes zero toward the plasma center, the χ_i value is small at the plasma center region. For this reason, different from the Dominguez & Waltz's case, the η_i value is large at the plasma center. As the η_{ic} value increases, the η_i value decreases at the plasma center and increases at the edge region because of the reason mentioned above. The calculated T_i profiles are almost the same and agree with experimental data for the different value of η_{ic}, although the shape of $f(\eta_i)$ is considerably different.

Next we examine the same matter on the high T_i plasma. In this case the second term of RHS of eq.(1) is eliminated. The result of Dominguez & Waltz's model with different η_{ic} value is shown in Fig.25. The C^{η_i} values are set 0.5, 0.5, 0.6 and 2.0 for the case of $\eta_{ic} = -\infty$, 1, 1.5 and 2, respectively which is the same with the L-mode case. As the η_{ic} value increases, in the plasma central region where the η_i value is essentially small comparing with that in the plasma edge region, the η_i mode becomes stabilized in the first place. It gives rise to the reduction of χ_i value in the plasma central region as the increase of η_{ic} value. Different from the L-mode case, the calculated T_i profile drastically changes as the increase of η_{ic} value. We can see better agreement between the calculated T_i and the experimental data with the higher η_{ic} value.

The same tendency is obtained for the Lee & Diamond's χ_i model. The calculation results is shown in Fig.26. The C^{η_i} values are set 2.5, 2.5, 3 and 10 for the case of $\eta_{ic} = -\infty$, 1, 1.5 and 2, respectively which is the same with the L-mode case. Since η_i value is small in the plasma central region, the η_i mode is easily stabilized there and the χ_i value decreases as the increase of η_{ic} value. As a result, the calculated T_i and the experimental data agree well in the higher η_{ic} value.

There are many formula of η_{ic} value but we cannot tell which is the conclusive one at the present time. At least for the high T_i plasmas in JT-60, the higher η_{ic} makes better agreement between the calculation and the experiment.

The ion temperature profiles of JT-60 neutral beam heated plasmas have been analyzed in the wide range of plasma parameters by using three different formula of χ_i model based on η_i mode turbulence. The calculated T_i profiles are compared with experimental data measured by charge exchange recombination reaction.

The calculated T_i profiles in the L-mode plasmas show considerably good agreement with experimental data in the wide range of plasma parameter; $I_P = 1.0 \sim 1.8$ MA, $P_{abs} = 1.3 \sim 16.7$ MW , $\bar{n}_e = 1.2 \sim 5.0 \times 10^{19}$ m^{-3} for the divertor plasmas and $I_P = 2.0 \sim 2.7$ MA, $P_{abs} = 3.0 \sim 17.4$ MW, $\bar{n}_e = 1.5 \sim 6.5 \times 10^{19}$ m^{-3} for the limiter plasmas with the fixed coefficients, $C^{\eta_i} = 0.5$, $C^{TE} = 0.2$, and $C^{CE} = 0.2$ for Dominguez & Waltz's model. Good agreement between the calculated T_i and the experimental data can also be seen in the different formula of the η_i mode model; Lee & Diamond's model with $C^{\eta_i} = 2.5$ and Romanelli's model with $C^{\eta_i} = 0.8$.

In these calculations, the dominant conduction loss is caused by the η_i mode turbulence in the bulk plasma. The decrease of χ_i value by this model toward the plasma edge region because of the low temperature is compensated with χ_i by the trapped electron mode and the circulating electron mode which increases toward plasma surface. However the edge χ_i enhancement is not always necessary because the dominant energy loss mechanisms in the plasma edge region are the convection loss or the equi-partition loss or the charge exchange loss, not the conduction loss. For this reason, the calculated T_i profile without the trapped electron mode or the circulating electron mode does not make so much difference from the results with these modes. Only at the plasma edge region, the T_i profile becomes somewhat fat if these modes are not considered.

Inclusion of these modes makes better agreement between the calculation results and experimental data. However, the edge transport model is not necessary to be the trapped electron mode nor the circulating electron mode. A mode with which χ_i value becomes large enough to compensate the decrease of χ_i by the η_i mode turbulence at the plasma edge region will do. For example, INTOR type thermal diffusivity is also available. We have also obtained the good agreement of calculated T_i with experimental data by using eq.(2) with the coefficient of $C^{INTOR} = 0.6$. In this case, the second term of RHS of eq.(2) is large near the plasma surface and decreases toward the plasma center like the case of TE/CE model. The η_i mode contribution to χ_i is also dominant conduction loss in the core plasma region all the same. This means that if we select the thermal diffusivity model which becomes large enough toward the plasma peripheral region to compensate the reduction of χ^{η_i} value, it does not matter whatever this additional χ_i model is.

In the 1.0 MA limiter plasmas, on the other hand, the calculated T_i becomes much higher than that of experimental data. The calculated χ_i is smaller than χ_i^{Scoop} by factor 4. There are two possibility to explain this discrepancy. One is that local χ_i strongly depends on I_p in the limiter plasmas whereas weakly depends on I_p in the divertor plasmas. In this case, the χ_i model mentioned above cannot explain the experimental T_i because there is essentially no I_p dependence in the χ_i formula in these models. The other possibility is that the ion density dilution due to the large Z_{eff} value can affect the calculation results. However, there are only three 1.0 MA data available and the much impurity background in the limiter case degrades the precision of T_i measurement. We cannot definitely conclude on this matter at the present time.

In the high T_i shot cases, the calculated T_i profiles becomes broader ones comparing with the experimental data which is pedestal and center peaked profile. Other transport mechanism, an inward heat pinch for example, must be considered in the plasma central region in order to explain the experimental data.

ACKNOWLEDGEMENT

The authors wish to express appreciation to Drs. K. Shimizu, T. Takizuka, M. Kikuchi, M. Nagami and K. Tani for fruitful discussions. The continuous encouragement of Drs. M. Yoshikawa, S. Tamura, Y. Shimomura is gratefully acknowledged.

REFERENCES

[1] H. Shirai, T. Hirayama, K. Shimizu, T. Takizuka, M. Azumi, Nucl. Fusion, **29** (1989) 805
[2] T. Hirayama, K. Shimizu, M. Kikuchi, H. Shirai, Transport Analysis of OH and NBI Heated Discharges in JT-60, Rep. JAERI-M 87-029, Japan Atomic Energy Research Institute (1987)
[3] JT-60 Team, Review of JT-60 Experimental Results from June to October 1988, Rep. JAERI-M 89-033, Japan Atomic Energy Research Institute (1988) p. 243
[4] R. R. Dominguez, R. E. Waltz, Nucl.Fusion, **27** (1987) 65.
[5] M. H. Redi, W. M. Tang, P. C. Efthimion, D. R. Mikkelsen, G. L. Schmidt, Nucl. Fusion, **27** (1987) 2001
[6] G. S. Lee, P. H. Diamond, Phys. Fluids, **29** (1986) 3291.
[7] F. Romanelli, Phys. Fluids, **B1** (1989) 1018
[8] C. S. Chang, F. L. Hinton, Phys. Fluids, **29** (1987) 3314.
[9] P. Terry, W. Anderson, W. Horton, Nucl. Fusion, **22** (1982) 487
[10] T. Hirayama, K. Shimizu, K. Tani, H. Shirai, M. Kikuchi, Experimental Transport Analysis Code System in JT-60, Rep. JAERI-M 88-043, Japan Atomic Energy Research Institute (1988)
[11] O. Naito, N. Hosogane, S. Tsuji, K. Ushigusa, H. Yoshida and JT-60 Team, Nucl. Fusion, **30** (1990) 195.

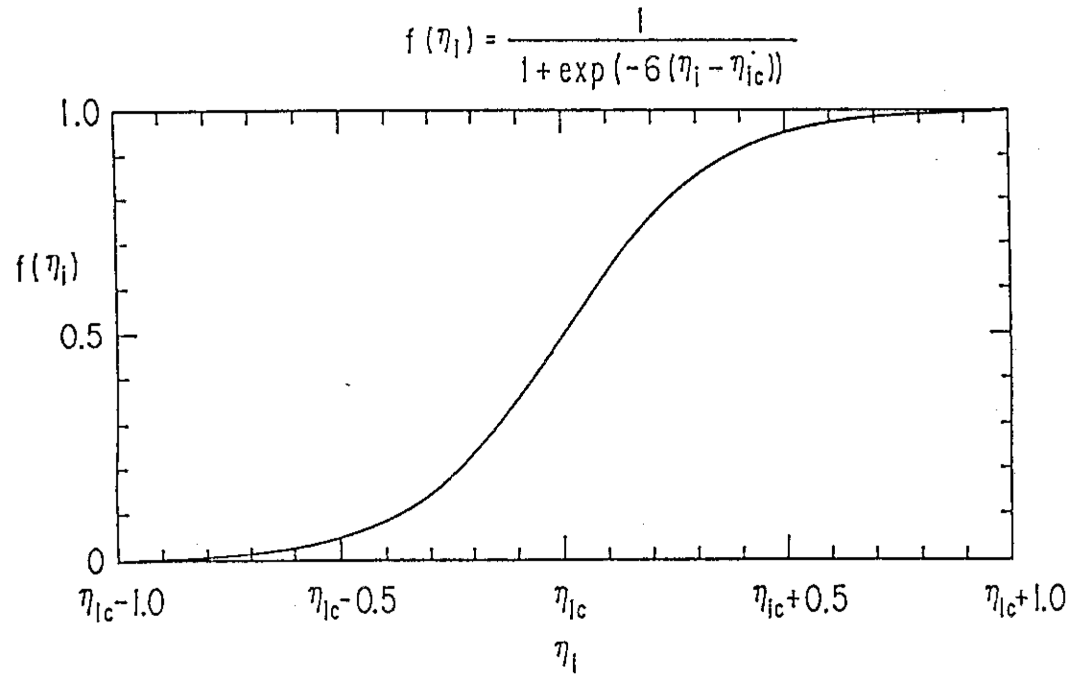

Fig.1 The profile of η_i mode on/off function, $f(\eta_i) = 1 / \{ 1 + \exp(-6(\eta_i - \eta_{ic})) \}$.

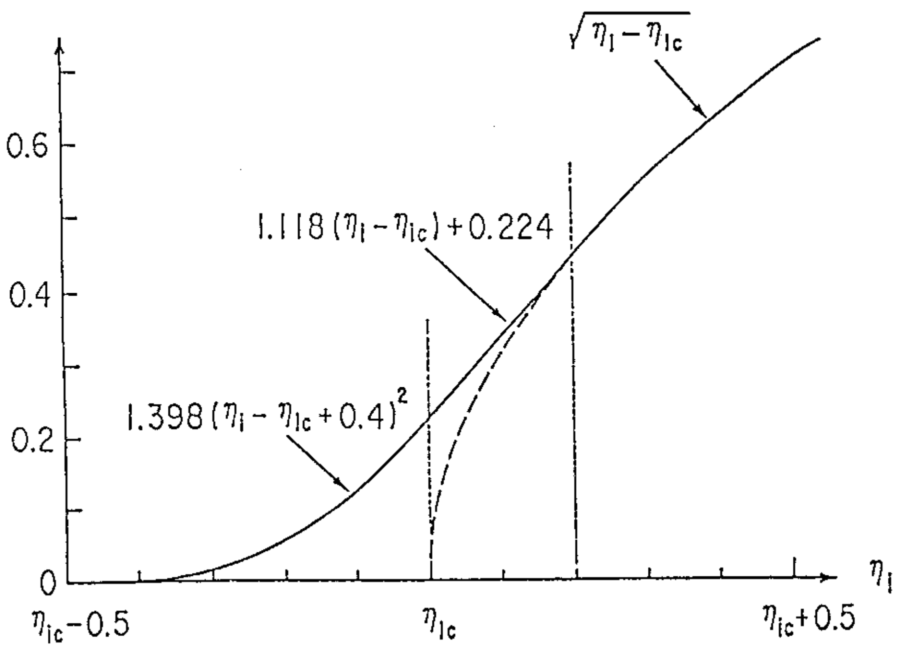

Fig.2 The original η_i dependence on χ_i of Romanelli's model (broken line) and the modified one we use in the calculation (solid line).

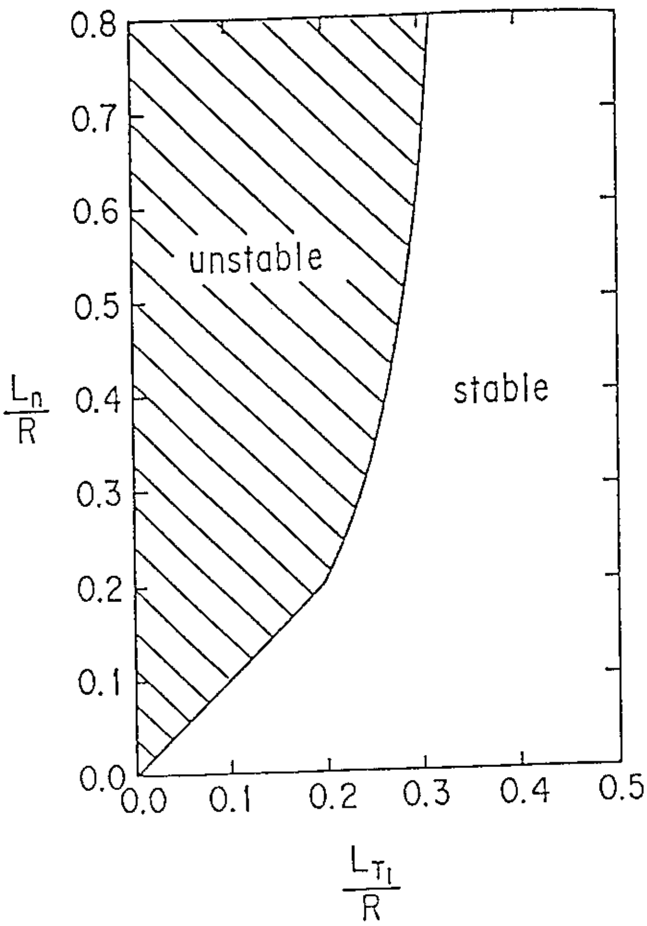

Fig.3 The unstable region against η_i mode in the (L_{T_i}, L_n) plane proposed by Romanelli.

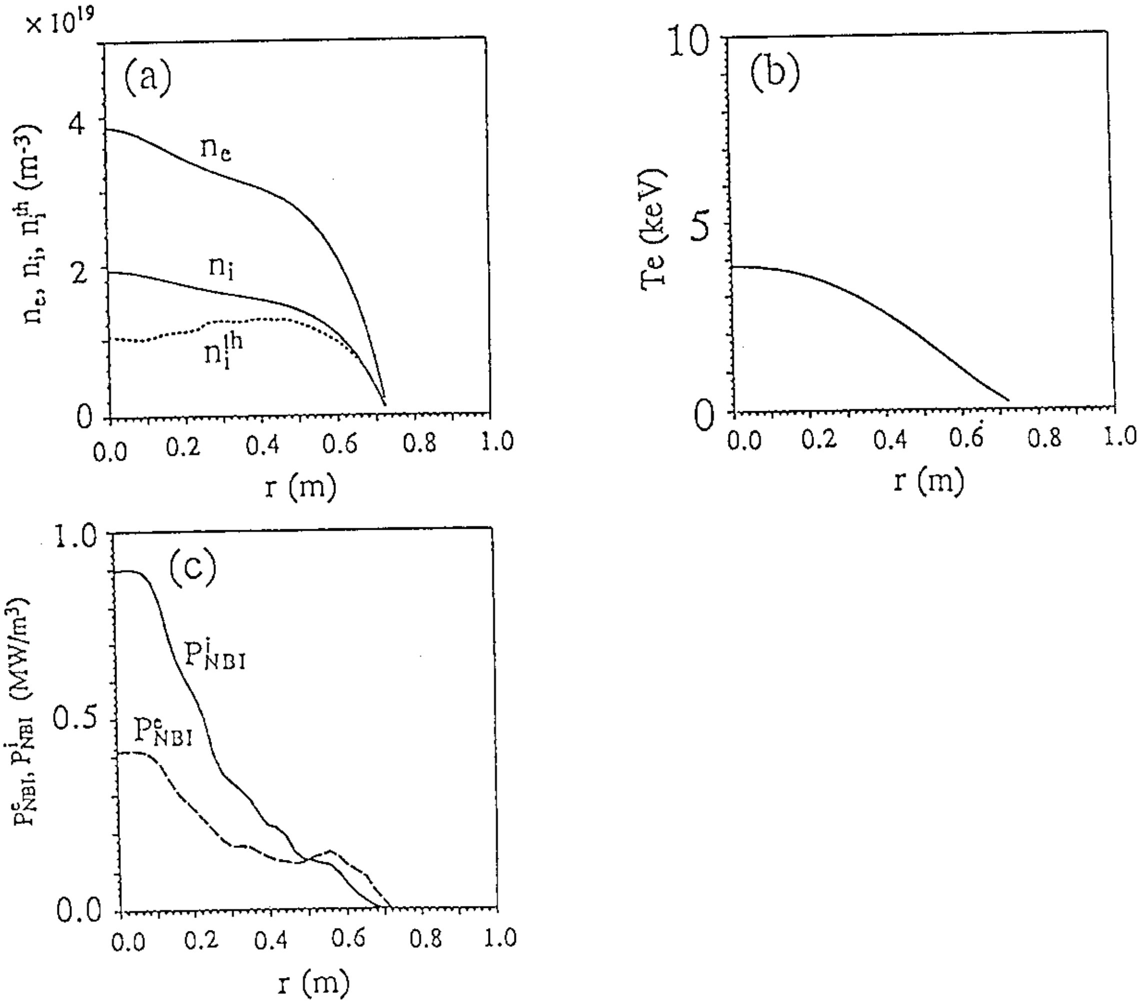

Fig.4 The profile of (a) n_e, n_i, n_i^{th}, (b) T_e measured by laser Thompson scattering and (c) P_{NBI}^e and P_{NBI}^i calculated by OFMC in the 1.5 MA divertor shot (E10737).

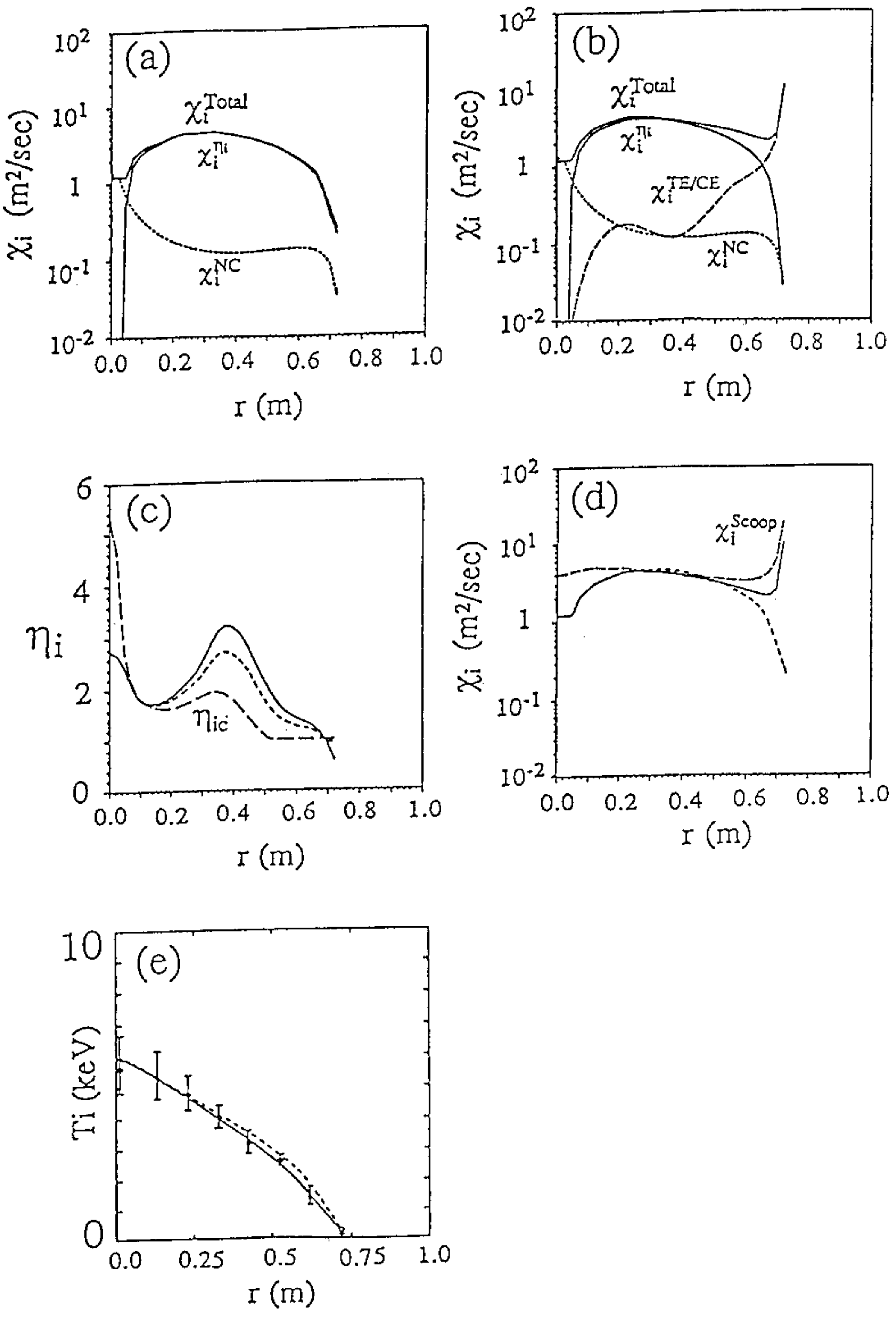

Fig.5 The profile of (a) calculated χ_i and its composition in case(I) (without edge transport model) and (b) calculated χ_i and its composition in case(II) (with edge transport model), (c) comparison of η_i value of case(I) (dotted line), case(II) (solid line) and η_{ic} (broken line), (d) comparison of χ_i of case(I) (dotted line), case(II) (solid line) and χ_i^{Scoop} (broken line), (e) comparison of calculated T_i of case(I) (dotted line), case(II) (solid line) and T_i^{Exp} in E10737. The calculated T_i profile of case(II) shows good agreement with experimental data.

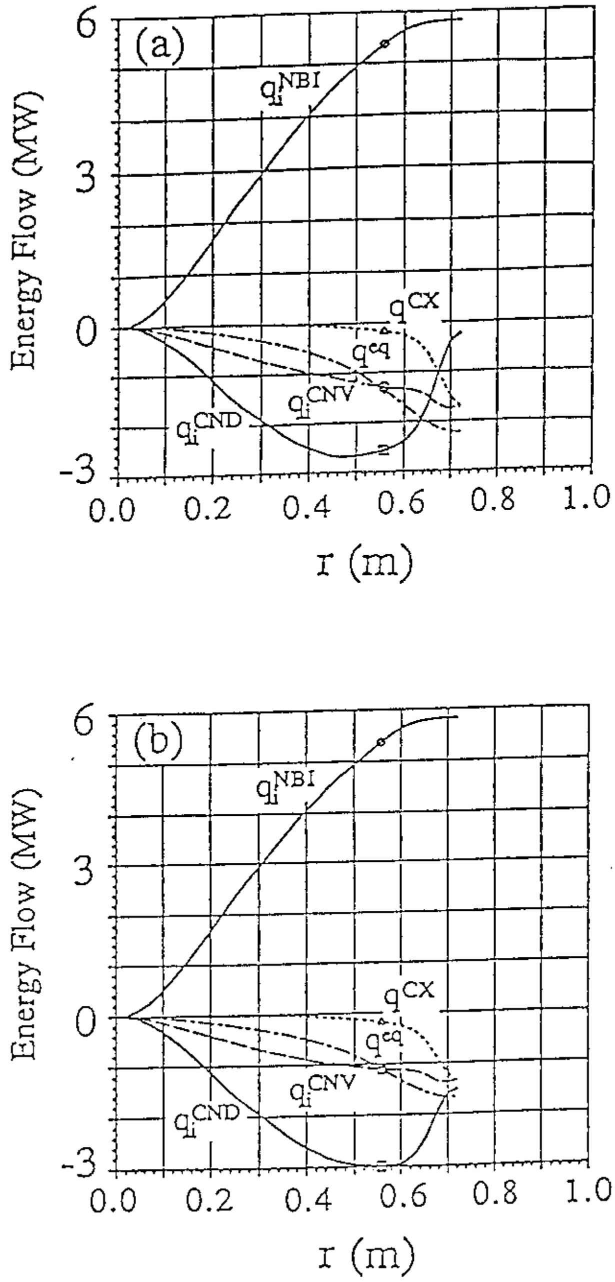

Fig.6 The energy flow integrated from the plasma center; the neutral beam input power (thin solid line), the conduction loss (thick solid line), the convection loss (broken line), the equi-partition loss (dotted-broken line) and the charge exchange loss (dotted line) of case (I) (Fig.(a)) and case(II) (Fig.(b)) in E10737.

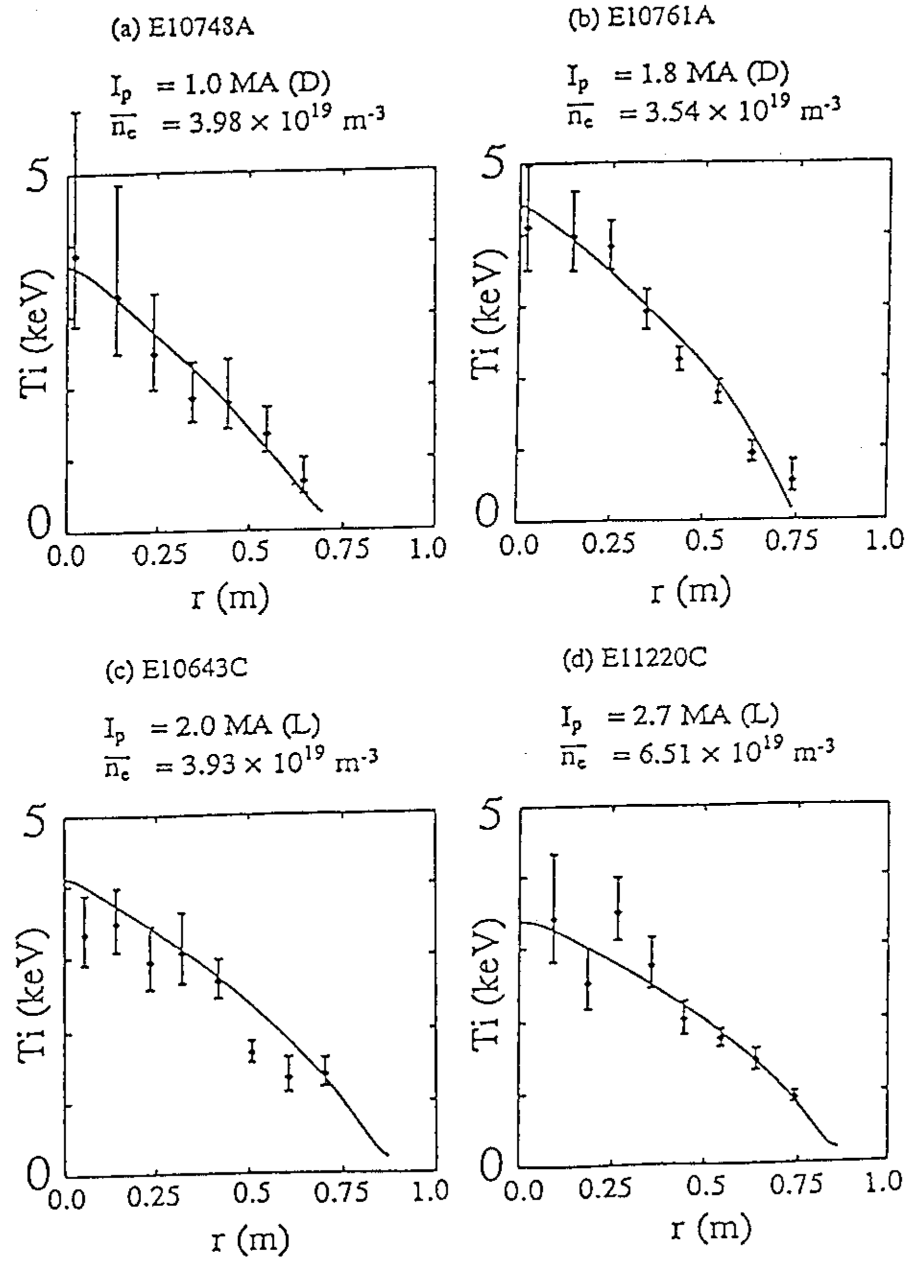

Fig.7 Comparison of calculated T_i profiles with T_i^{Exp} in the different plasma current of (a) 1.0 MA divertor, (b) 1.8 MA divertor, (c) 2.0 MA limiter and (d) 2.7 MA limiter. The absorption power is 9.7 ~ 12.1 MW. They show good agreement.

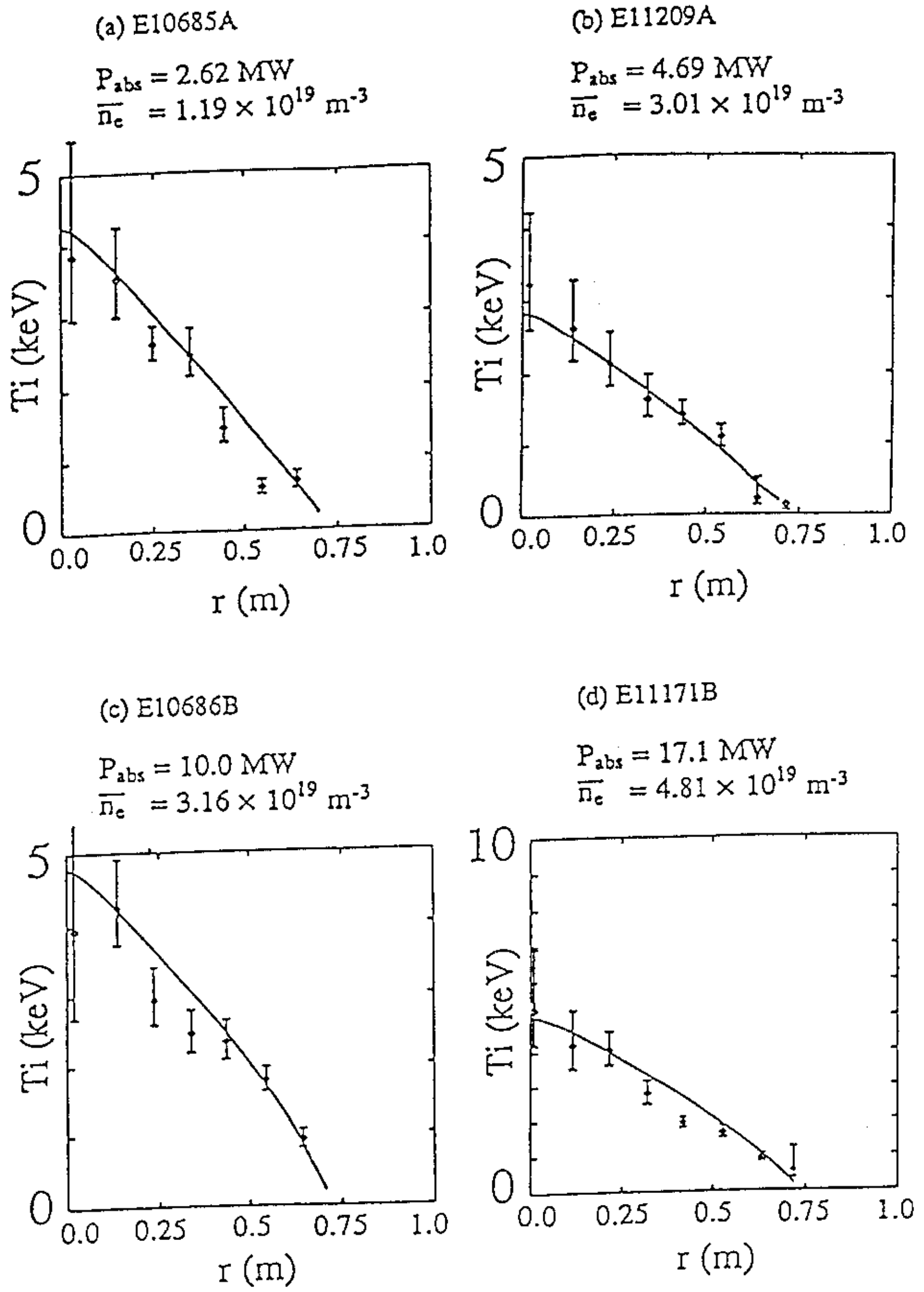

Fig.8 Comparison of calculated T_i profiles with T_i^{Exp} in 1.0 MA divertor shots with different absorption power. The T_i profiles show good agreement.

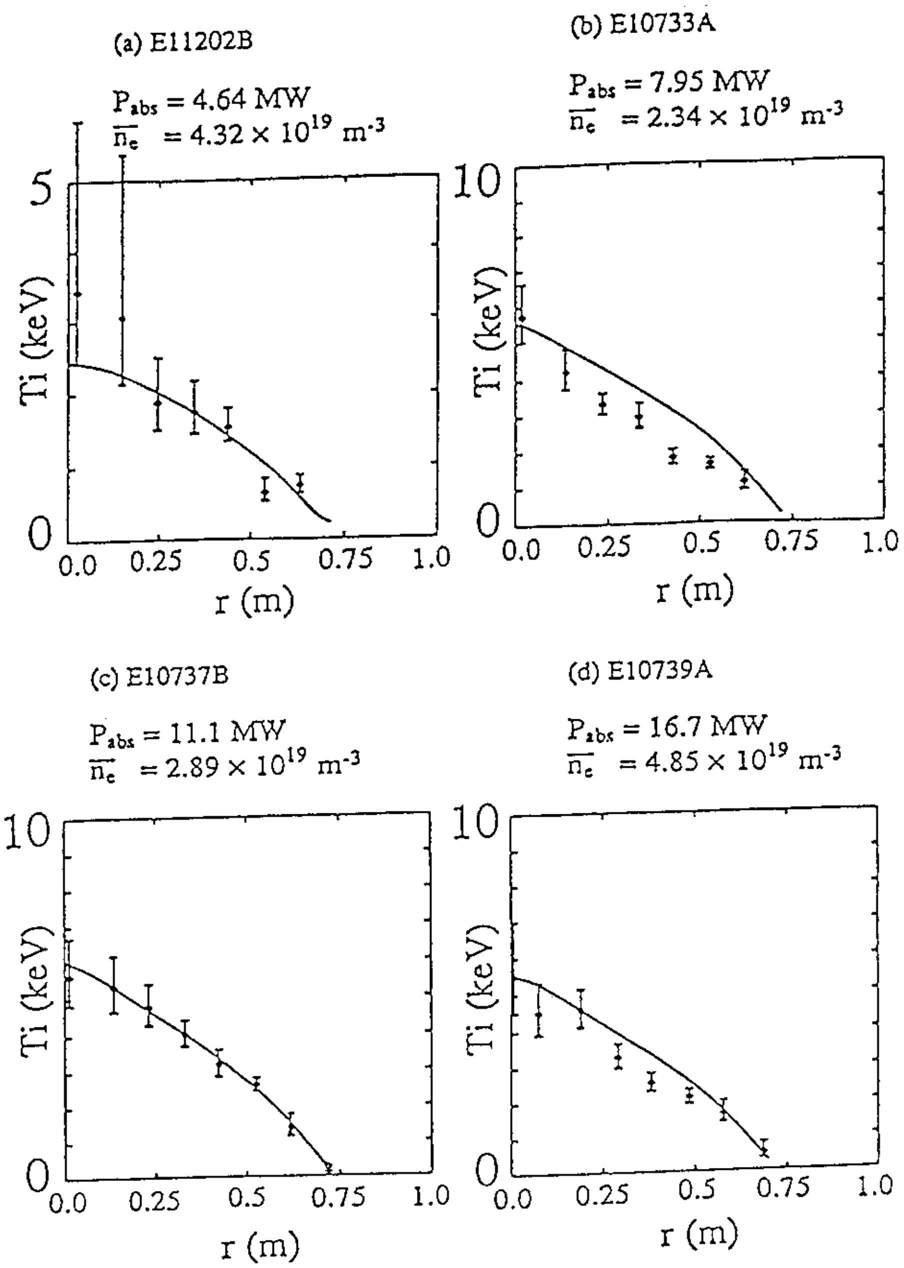

Fig.9 Comparison of calculated T_i profiles with T_i^{Exp} in 1.5 MA divertor shots with different absorption power. The T_i profiles show good agreement.

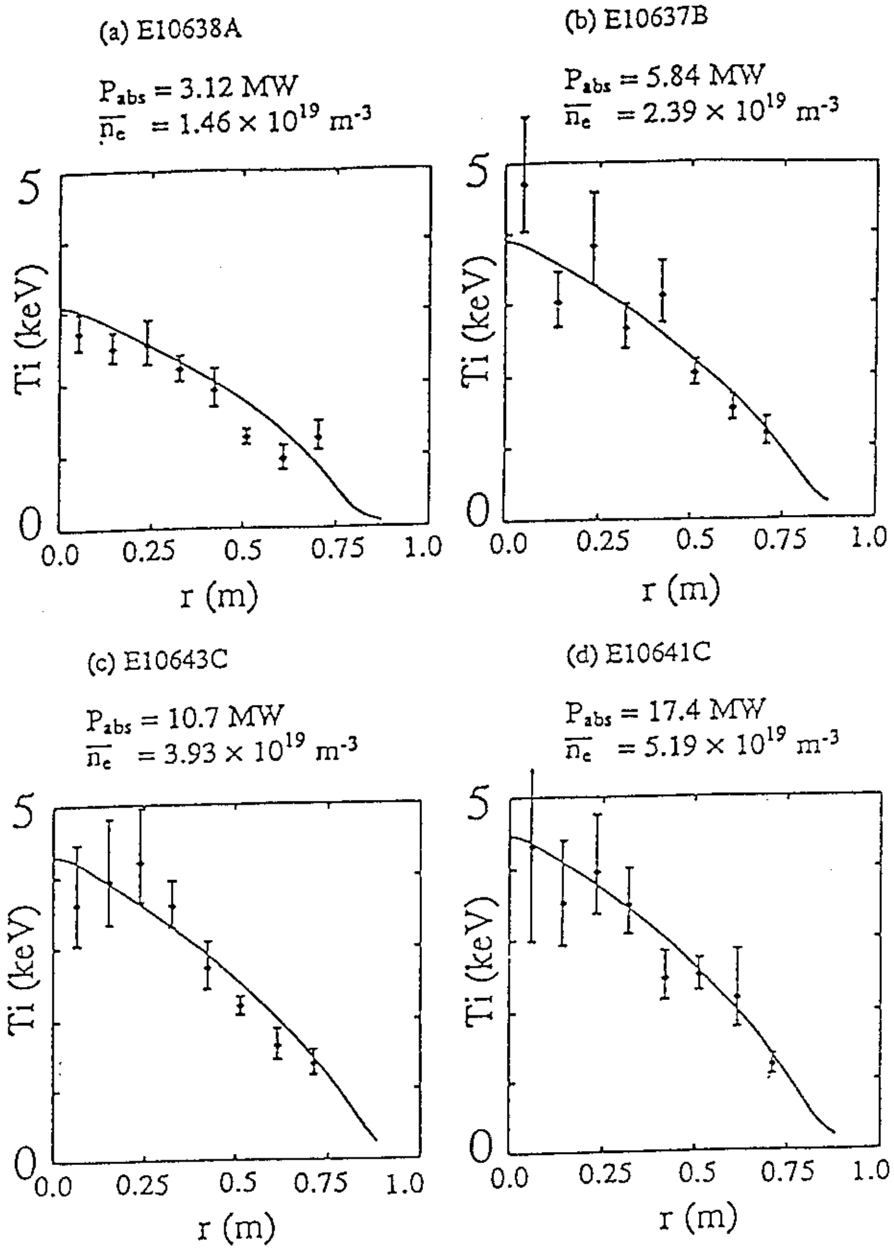

Fig.10 Comparison of calculated T_i profiles with T_i^{Exp} in 2.0 MA limiter shots with different absorption power. The T_i profiles show good agreement.

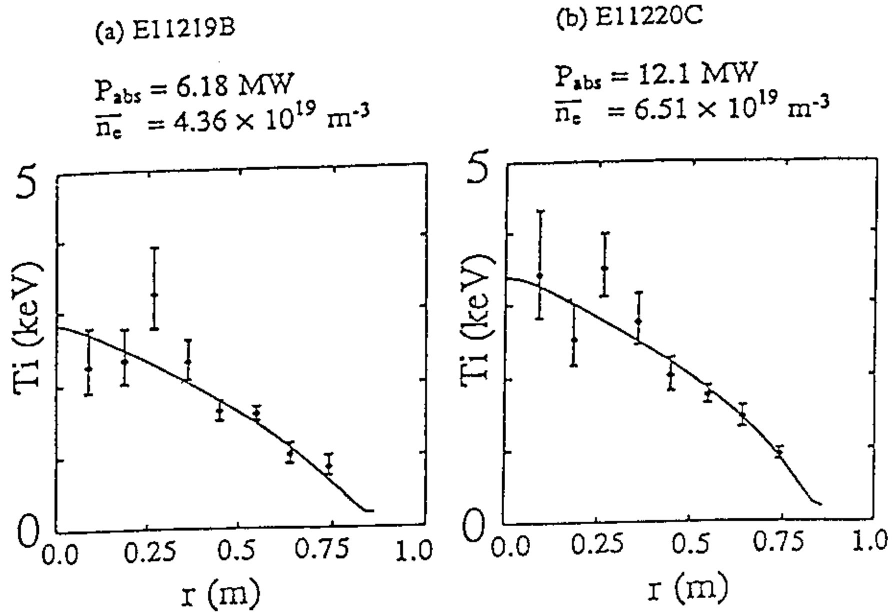

Fig.11 Comparison of calculated T_i profiles with T_i^{Exp} in 2.7 MA limiter shots with different absorption power. The T_i profiles show good agreement.

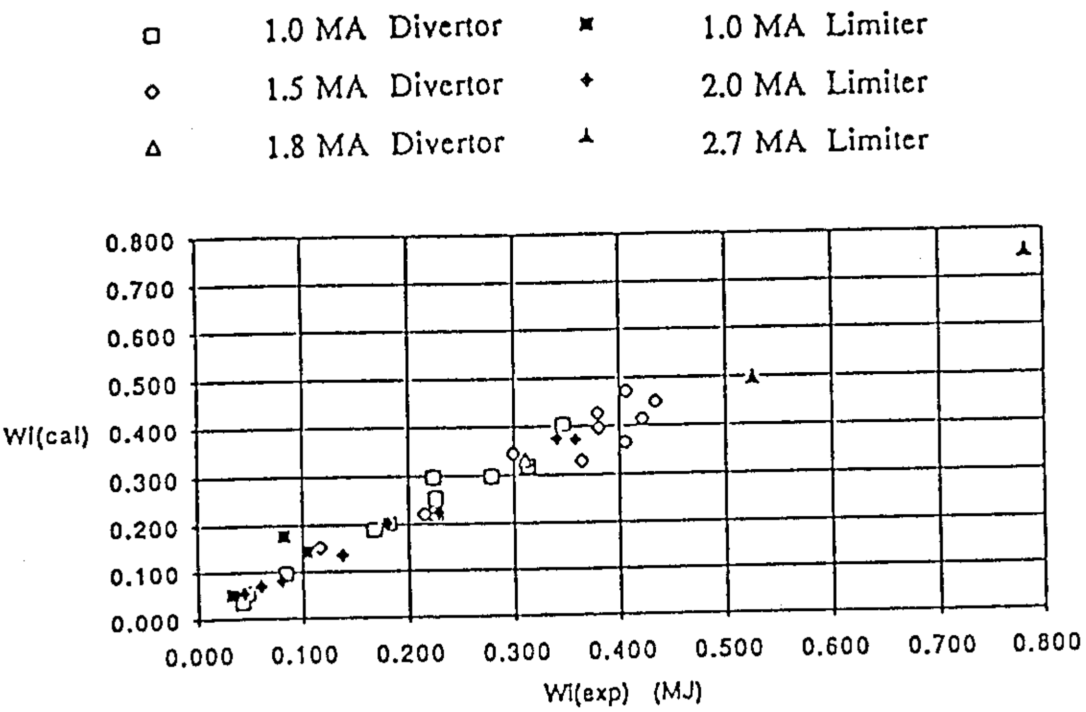

Fig.12 Comparison of ion stored energy by calculation with that of experimental data. They show good agreement except for some 1.0 MA limiter shots.

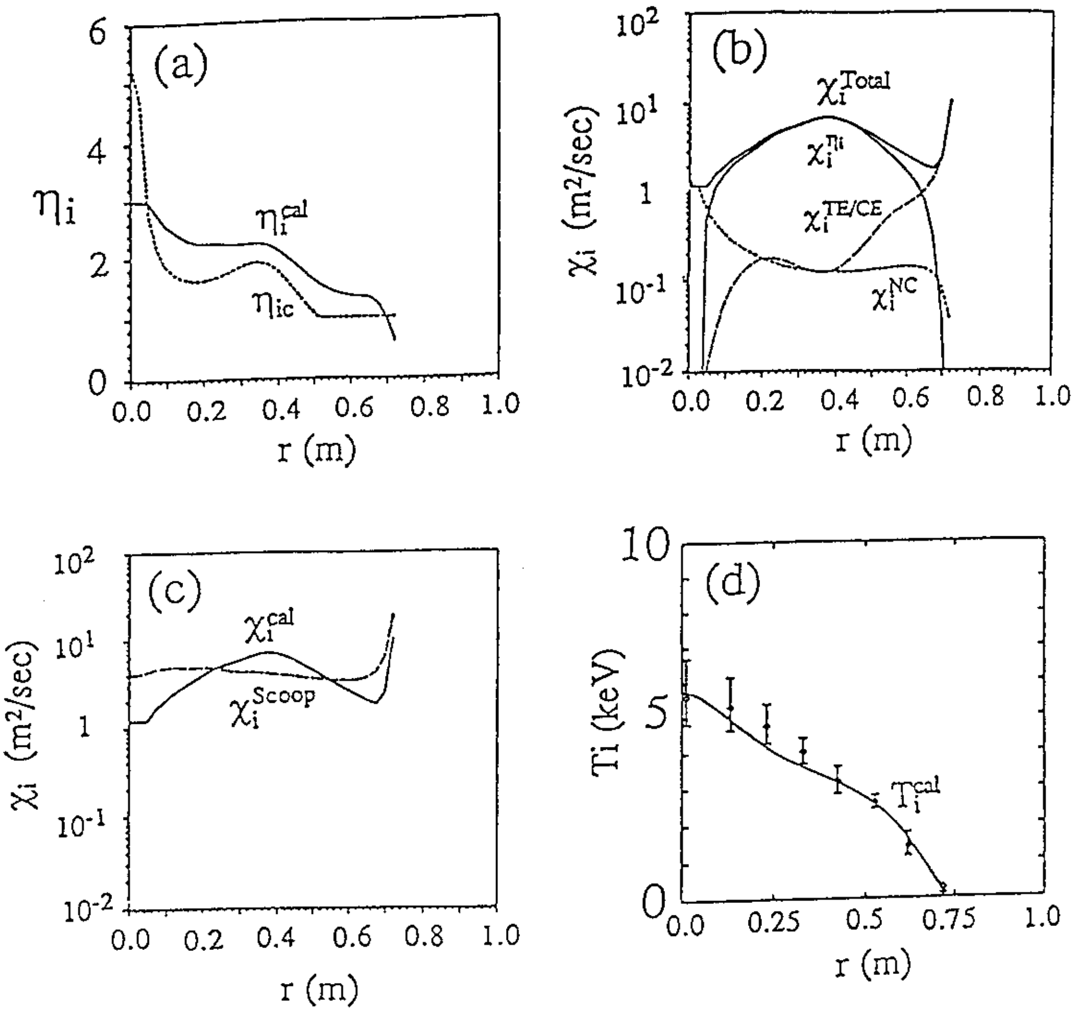

Fig.13 The profile of (a) η_i (solid line) and η_{ic} (dotted line), (b) χ_i and its composition, (c) χ_i (solid line) with χ_i^{Scoop} (broken line), (d) comparison of calculated T_i with T_i^{Exp} in E10737 with Lee & Diamond's χ_i model.

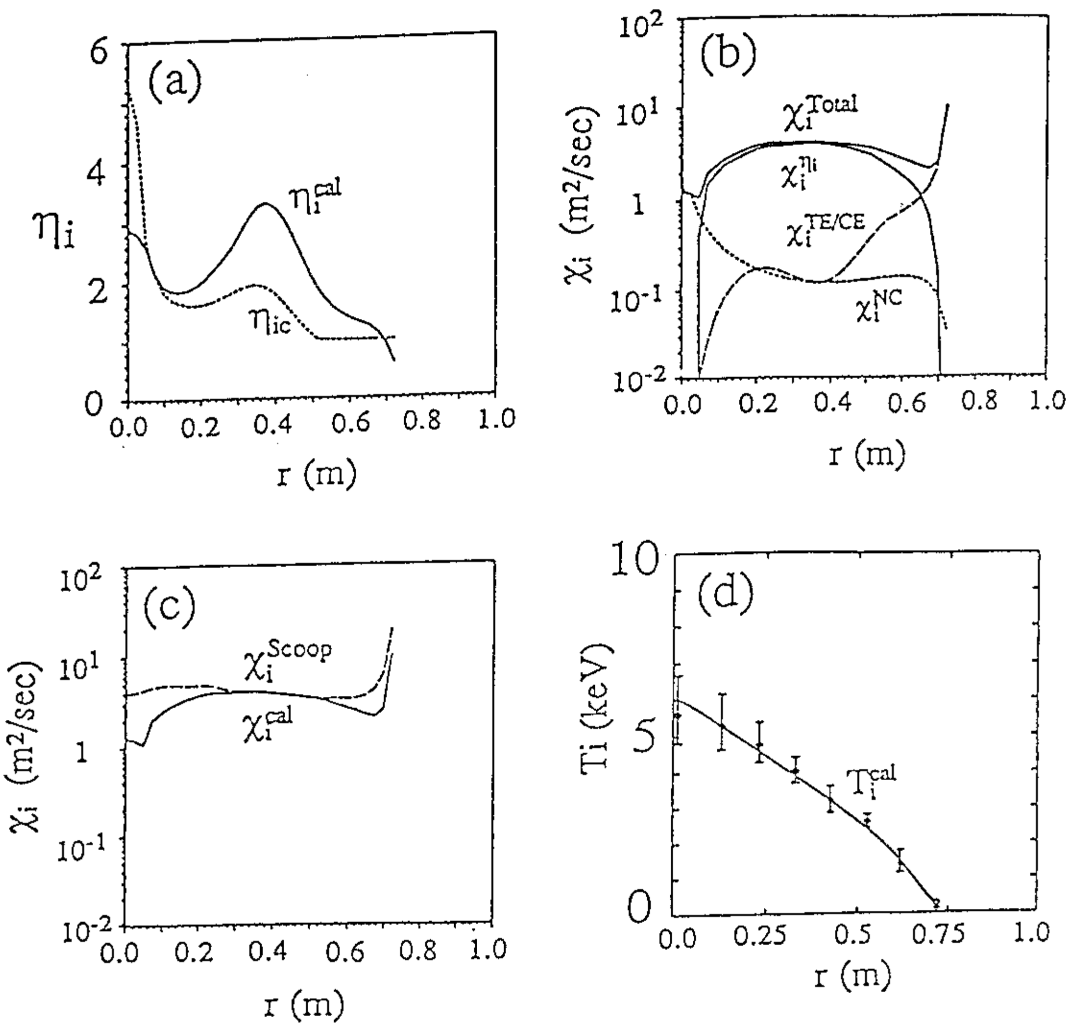

Fig.14 The profile of (a) η_i (solid line) and η_{ic} (dotted line), (b) χ_i and its composition, (c) χ_i (solid line) with χ_i^{Scoop} (broken line), (d) comparison of calculated T_i with T_i^{Exp} in E10737 with Romanelli's χ_i model.

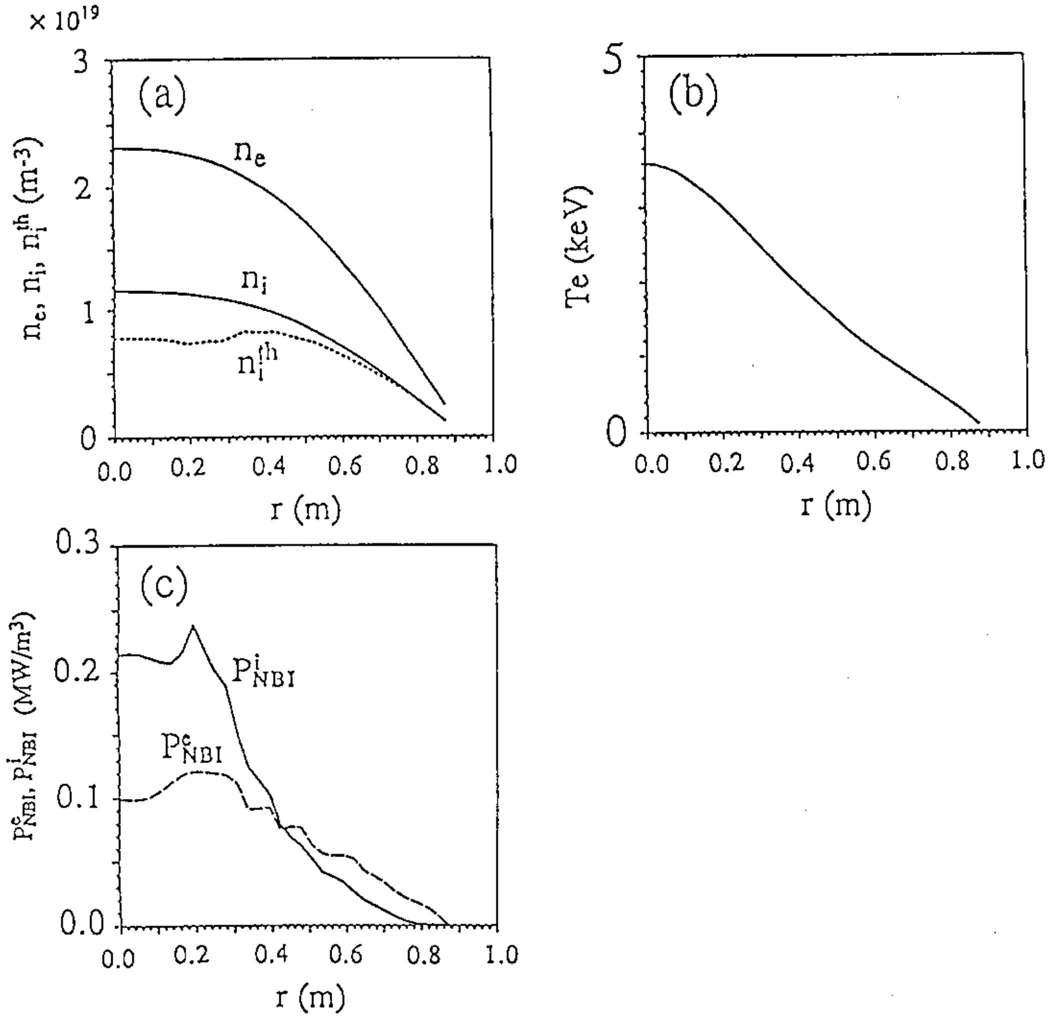

Fig.15 The profile of (a) n_e, n_i, n_i^{th}, (b) T_e measured by laser Thompson scattering, (c) P^e_{NBI} and P^i_{NBI} calculated by OFMC in the 1.0 MA limiter shot (E10619).

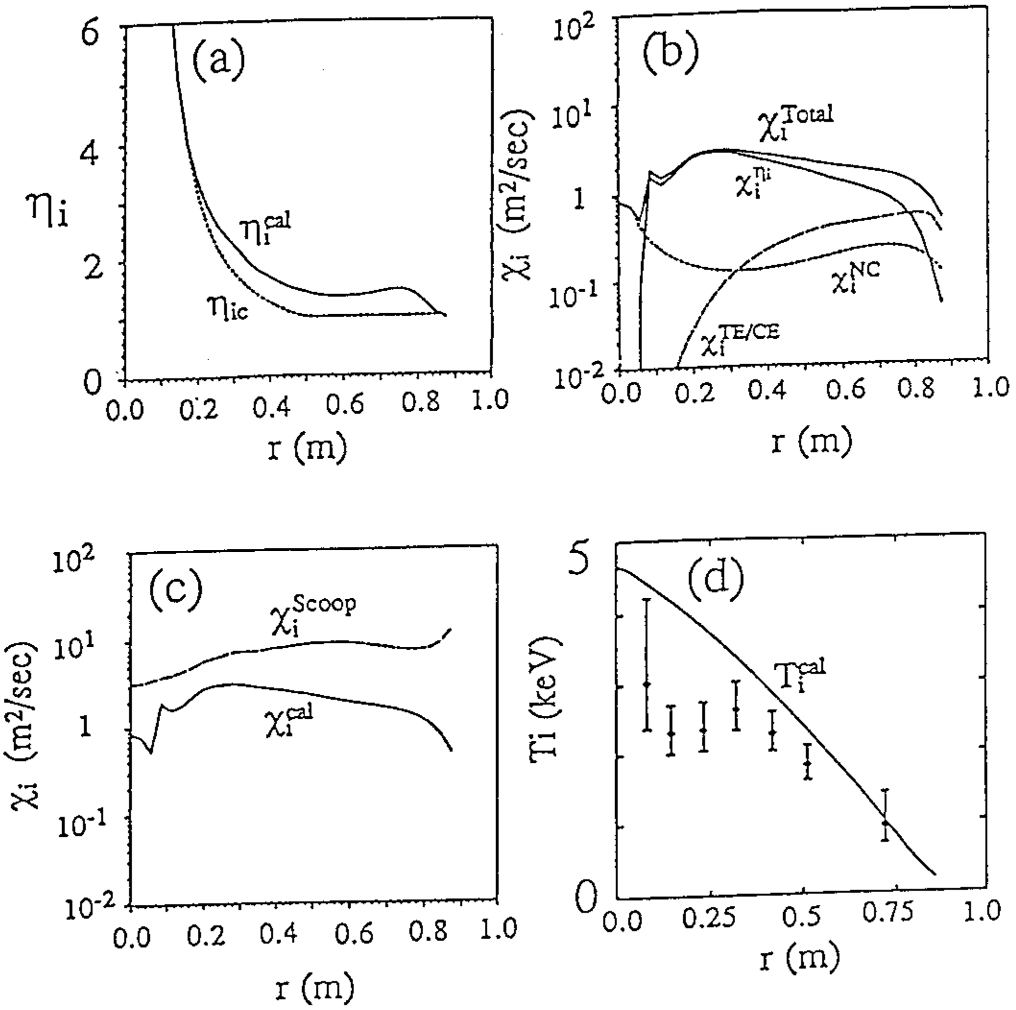

Fig.16 The profile of (a) η_i (solid line) and η_{ic} (dotted line), (b) χ_i and its composition, (c) comparison of χ_i (solid line) with χ_i^{Scoop} (broken line), (d) comparison of calculated T_i with T_i^{Exp} in E10619.

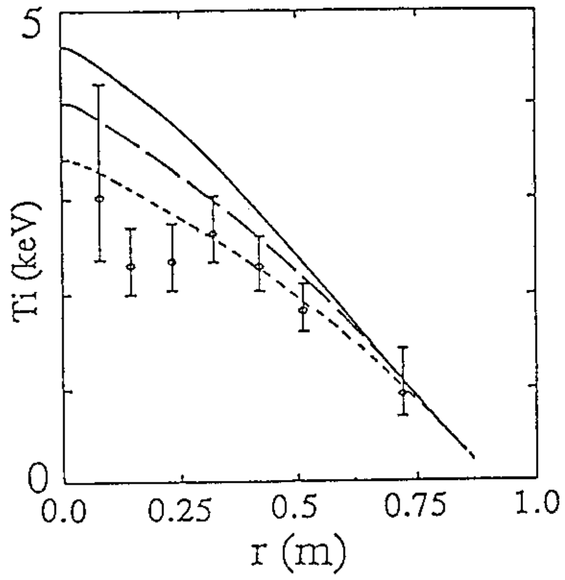

Fig.17 The profile of calculated T_i and T_i^{Exp} in E10619 with $(C^{\eta_i}, C^{TE}, C^{CE})$ = (0.5, 0.2, 0.2), (1.0, 0.4, 0.4) and (2.0, 0.8, 0.8). These are shown in the solid line, broken line and the dotted line, respectively.

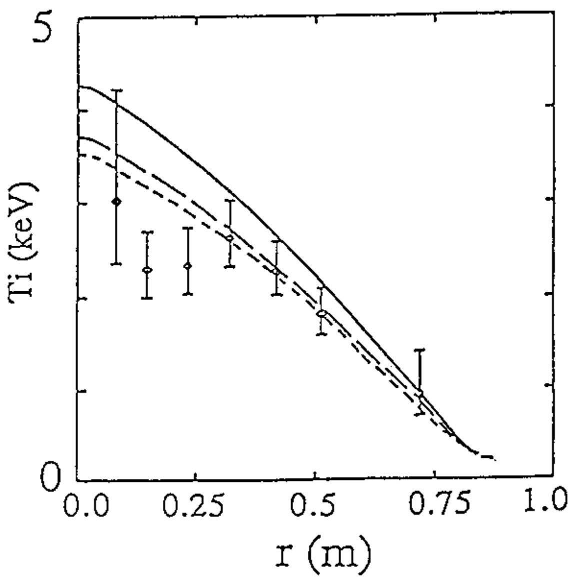

Fig.18 The profile of calculated T_i and T_i^{Exp} in E10619 with Z_{eff} = 3.0 (solid line), 2.0 (broken line) and 1.5 (dotted line).

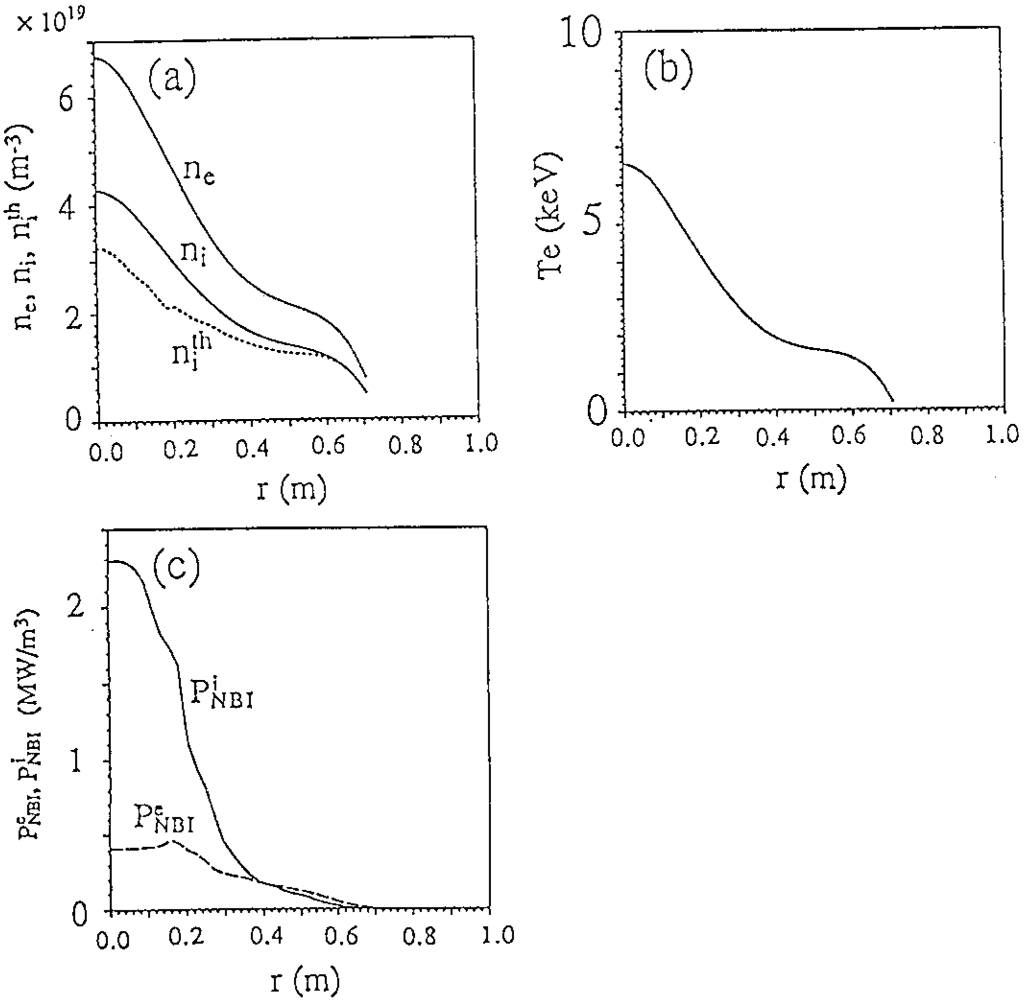

Fig.19 The profile of (a) n_e, n_i, n_i^{th}, (b) T_e measured by laser Thompson scattering, (c) P_{NBI}^e and P_{NBI}^i calculated by OFMC in the 0.5 MA high T_i shot (E10300).

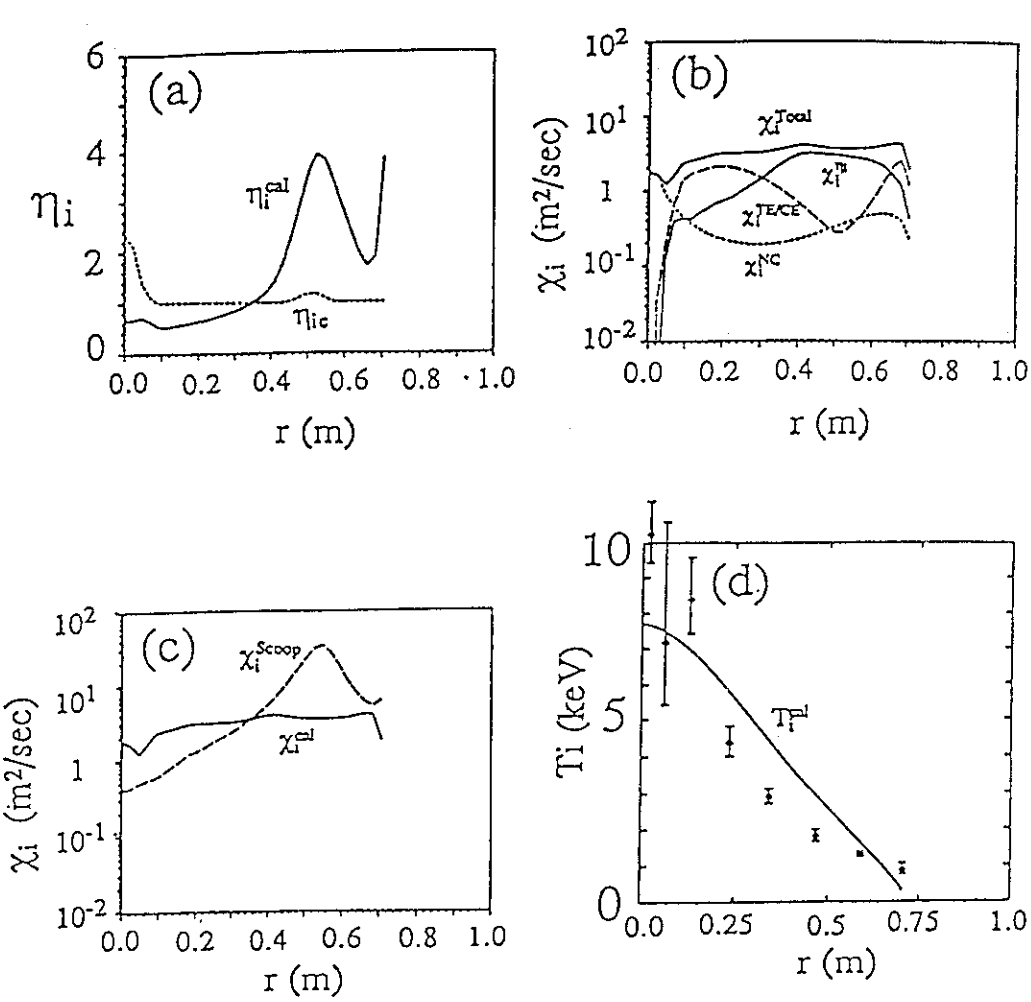

Fig.20 The profile of (a) calculated η_i, (b) χ_i and its composition, (c) comparison of χ_i (solid line) with χ_i^{Scoop} (broken line), (d) comparison of calculated T_i with T_i^{Exp} in E10300.

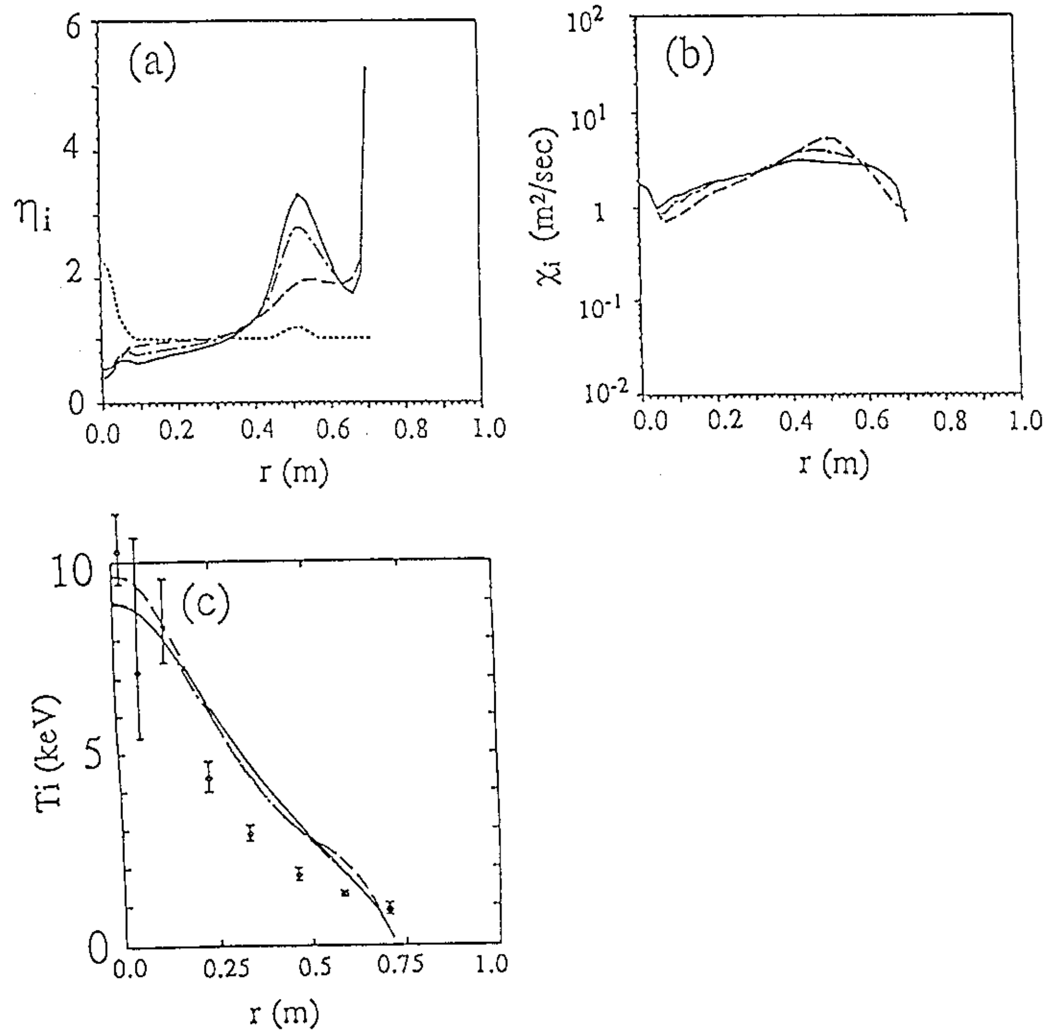

Fig.21 The profile of (a) η_i (solid line) and η_{ic} (dotted-line), (b) calculated χ_i and its composition, (c) comparison of calculated T_i with T_i^{Exp} in E10300 without edge transport model. The solid line, the broken line and dotted-broken line indicate χ_i model proposed by Dominguez, Lee and Romanelli respectively.

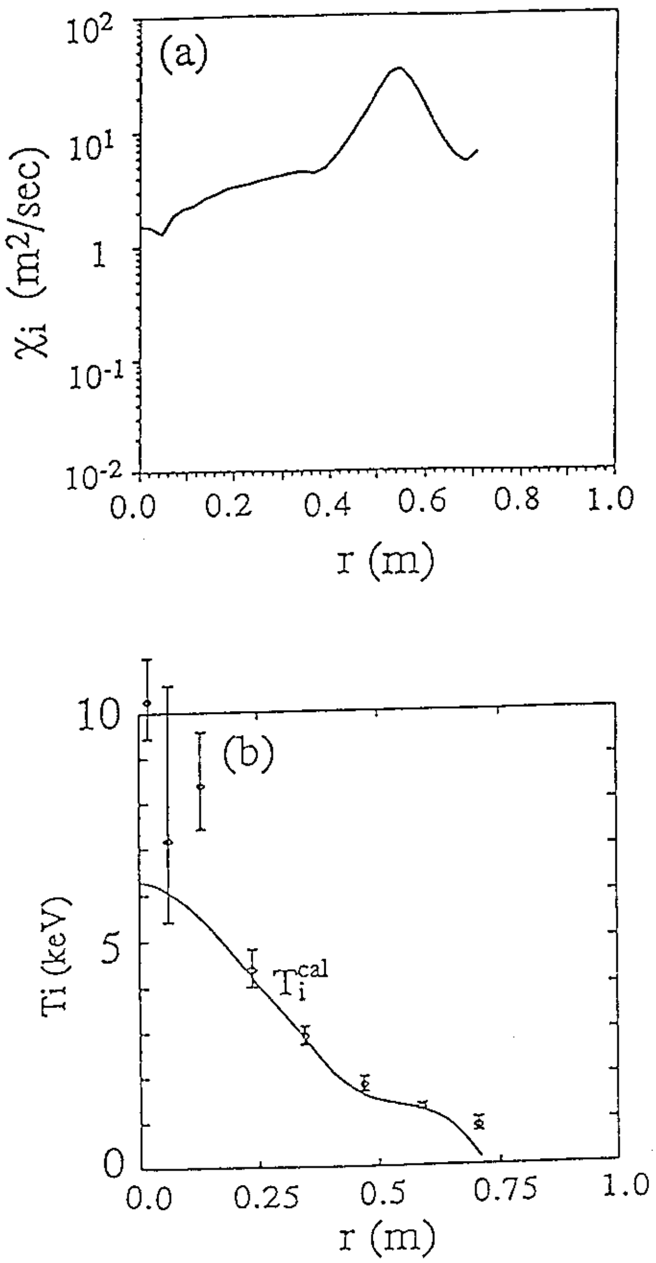

Fig.22 The profile of (a) χ_i and (b) comparison of T_i with T_i^{Exp} in E10300, in which χ_i model by η_i mode is effective only in the region of $\frac{r}{a} \leq \frac{1}{2}$. The calculated central T_i value is smaller than experimental data.

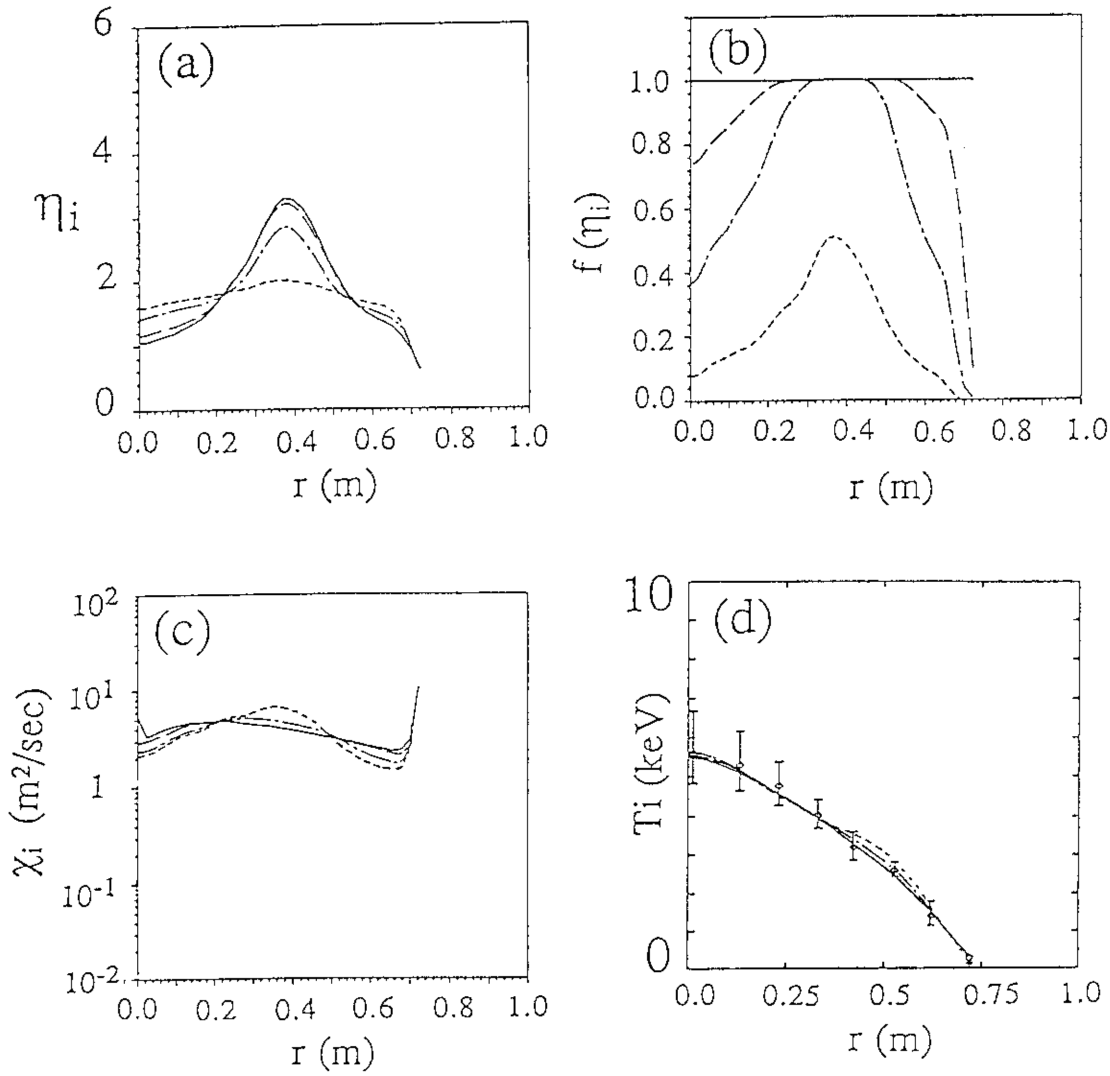

Fig.23 The profile of (a) η_i, (b) $f(\eta_i)$, (c) χ_i and (d) comparison of T_i with T_i^{Exp} in E10737 calculated by Dominguez & Waltz's model with the different value of η_{ic}. The solid line, the broken line, the dotted-broken line and the dotted line correspond to $\eta_{ic} = -\infty$, 1, 1.5 and 2 respectively. The C^{η_i} values are 0.5, 0.5, 0.6 and 2 respectively.

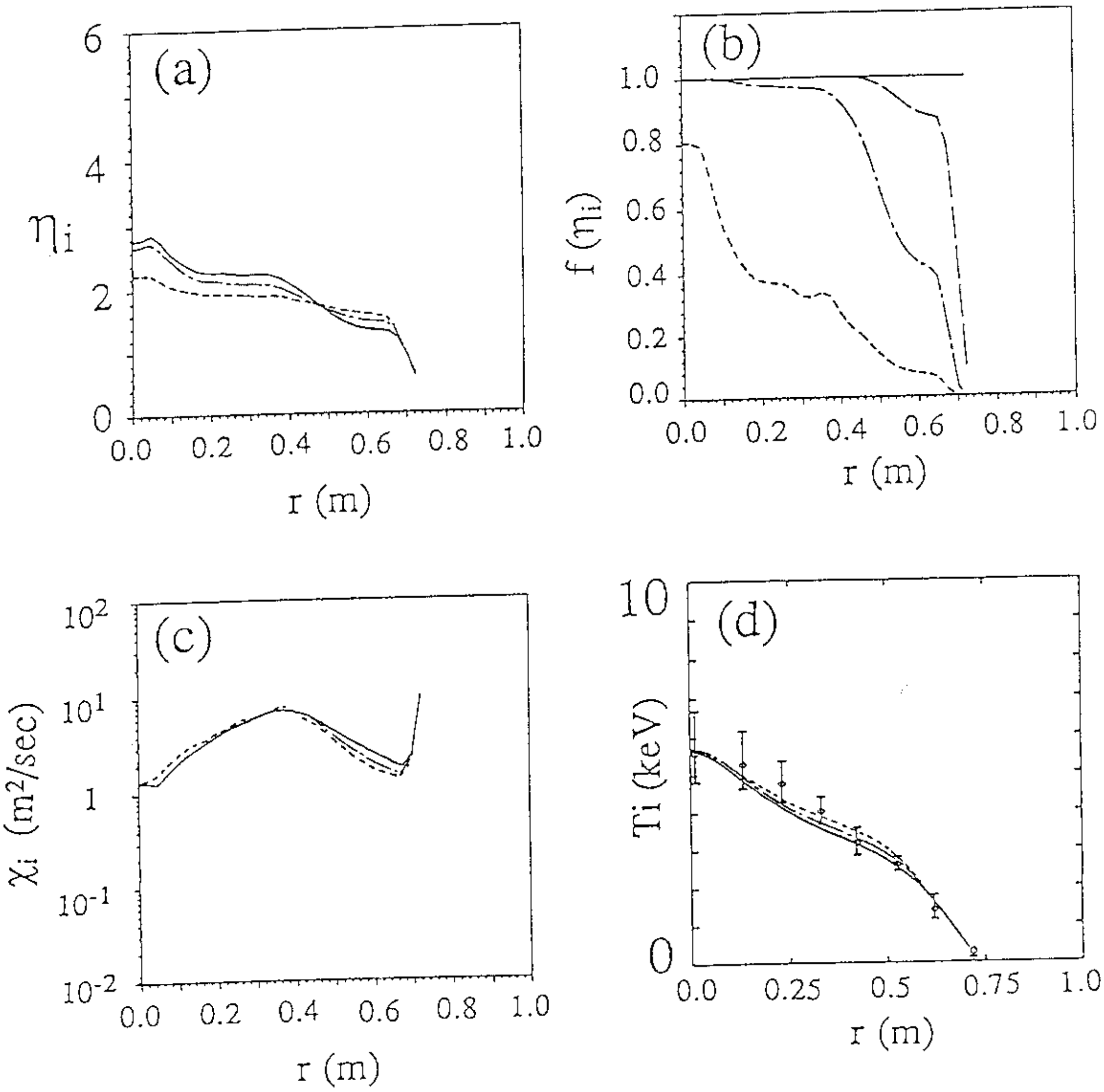

Fig.24 The profile of (a) η_i, (b) $f(\eta_i)$, (c) χ_i and (d) comparison of T_i with T_i^{Exp} in E10737 calculated by Lee & Diamond's model with the different value of η_{ic}. The solid line, the broken line, the dotted-broken line and the dotted line correspond to $\eta_{ic} = -\infty$, 1, 1.5 and 2 respectively. The C^{η_i} values are 2.5, 2.5, 3 and 10 respectively.

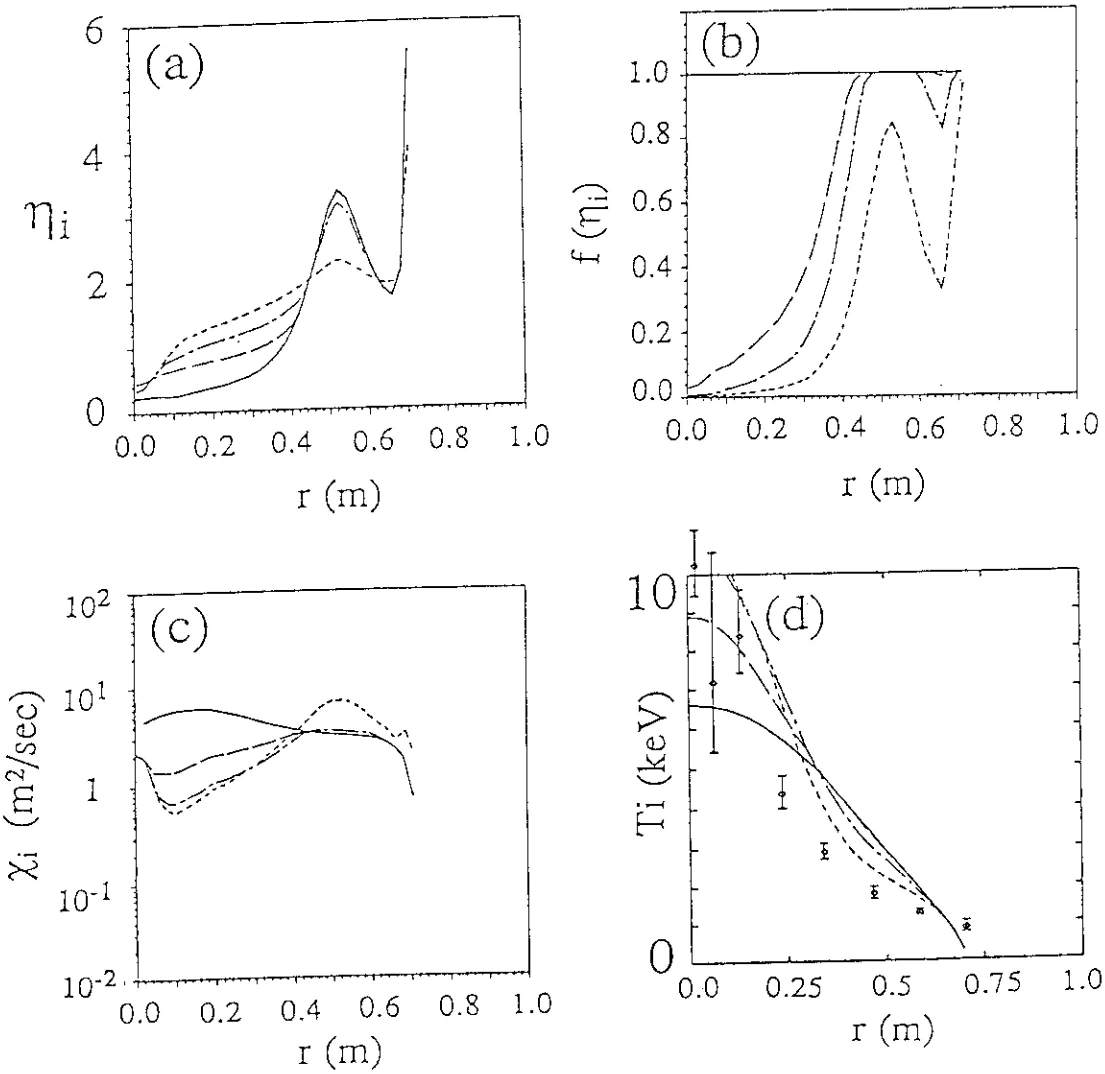

Fig.25 The profile of (a) η_i, (b) $f(\eta_i)$, (c) χ_i and (d) comparison of T_i with T_i^{Exp} in E10300 calculated by Dominguez & Waltz's model with the different value of η_{ic}. The solid line, the broken line, the dotted-broken line and the dotted line correspond to $\eta_{ic} = -\infty$, 1, 1.5 and 2 respectively. The C^{η_i} values are 0.5, 0.5, 0.6 and 2 respectively. The edge transport model is not adopted in this calculation.

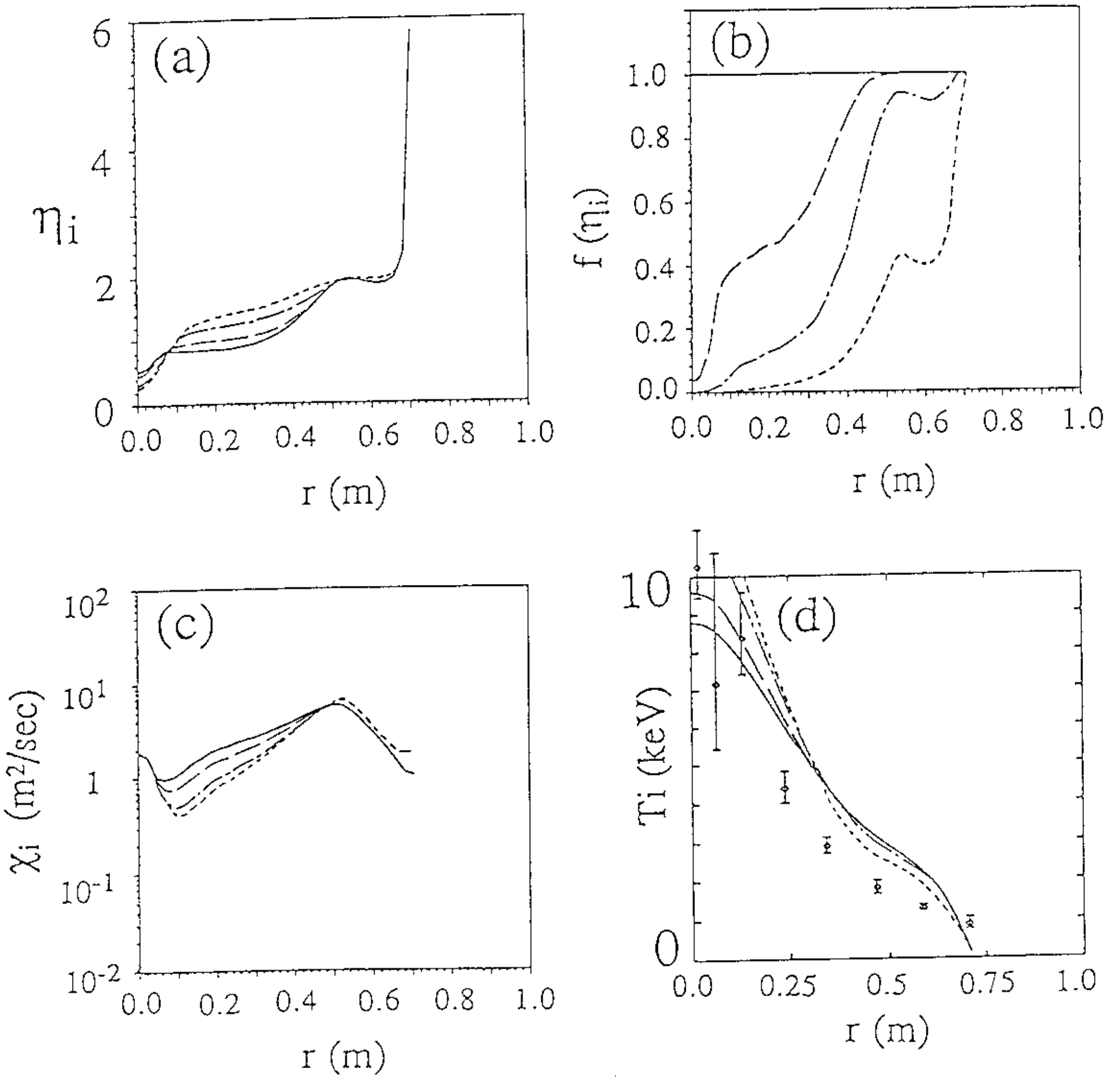

Fig.26 The profile of (a) η_i, (b) $f(\eta_i)$, (c) χ_i and (d) comparison of T_i with T_i^{Exp} in E10300 calculated by Lee & Diamond's model with the different value of η_{ic}. The solid line, the broken line, the dotted-broken line and the dotted line correspond to $\eta_{ic} = -\infty$, 1, 1.5 and 2 respectively. The C^{η_i} values are 2.5, 2.5, 3 and 10 respectively. The edge transport model is not adopted in this calculation.